

Tephra dispersal and composition reveal the explosive onset of a large basaltic fissure eruption: Timanfaya, Lanzarote, 1730–1736 CE

James K. Muller and Marc-Antoine Longpré*

*mlongpre@qc.cuny.edu

This is a non-peer reviewed preprint submitted to EarthArXiv in on August 2nd 2023.

Tephra dispersal and composition reveal the explosive onset of a large basaltic fissure eruption: Timanfaya, Lanzarote, 1730–1736 CE

James K. Muller^{1,2} and Marc-Antoine Longpré^{1,3*}

¹School of Earth and Environmental Sciences, Queens College, City University of New York, Queens, NY 11367, USA

²Scripps Institution of Oceanography, University of California San Diego, La Jolla, CA 92093, USA

³Earth and Environmental Sciences, The Graduate Center, City University of New York, New York, NY 10016, USA

*Corresponding author at: School of Earth and Environmental Sciences, Queens College, City University of New York, Queens, New York 11367, USA.

E-mail address: mlongpre@qc.cuny.edu (M.-A. Longpré)

ABSTRACT

Basaltic fissure eruptions are chiefly characterized by sizable emissions of lava flows and volcanic gases, posing significant hazards. However, such eruptions may be punctuated by explosive episodes, which are comparatively poorly understood but may have important volcanic hazard and environmental implications. The 1730–1736 CE Timanfaya eruption on Lanzarote, Canary Islands, is a large basaltic fissure eruption characterized by a marked temporal–compositional trend from early basanite to late tholeiite lavas, but little is known on its associated pyroclastic deposits. Here we report field and geochemical data from the tephra deposits of the Timanfaya eruption to reconstruct eruptive style over time. Stratigraphic sections demonstrate the wide dispersal of the tephra blanket, with a bulk volume of $\sim 0.44 \text{ km}^3$. We find that nearly all distal tephra are characterized by low SiO_2 content and high incompatible trace element concentrations that only match the compositions of tephra sourced from vents active in the eruption's initial phase. This implies that violent explosive activity was restricted to the first few months of activity, followed by prolonged, dominantly effusive eruptive style. Isopleth data from a basal tephra layer suggest that eruption columns lofted to $\geq 8 \text{ km}$ altitude. Explosive activity at Timanfaya was thus similar to that of the 1783–1784 Laki and 2021 Cumbre Vieja eruptions, highlighting the explosive potential of mafic volcanism in the Canary Islands. Our data suggest that early basanitic magmas were particularly volatile-rich and reveal a correlation between magma composition and eruptive style, although a causative link remains untested. We infer that the Timanfaya eruption released 11–26 Tg of sulfur (and 81–431 Tg CO_2) to the atmosphere, but ice core evidence for stratospheric transport of sulfur is unclear. Yet, a number of climate proxy records suggest that the eruption had significant hemispheric climate and environmental consequences. For large-volume basaltic eruptions characterized by effusive and explosive eruptive styles, such as Laki and Timanfaya, Volcanic Explosivity Index values appear most representative of associated hazards and impacts when based on eruptive volume estimates.

KEYWORDS

Basaltic fissure eruptions, eruptive style, tephra stratigraphy, Lanzarote, Timanfaya

INTRODUCTION

Large basaltic fissure eruptions pose significant hazards, mostly through massive emissions of lava flows and volcanic gases that can negatively impact the environment. Recent examples include the 2014–2015 Holuhraun eruption, Iceland (Gudmundsson et al., 2016), and the 2018 Lower East Rift Zone eruption of Kilauea volcano, Hawaii (Neal et al., 2019), but perhaps the best-known case is the 1783–1784 CE Laki eruption, in Iceland (Thordarson & Self, 1993, 2003). The Laki eruption produced a huge lava flow field, some 599 km² in area and 14.7 km³ in volume, from a 27-km-long fissure and it released ~304 Tg CO₂, 122 Tg SO₂, 7 Tg HCl and 15 Tg HF to the atmosphere, leading to adverse environmental effects particularly acute in Iceland but felt across the Northern Hemisphere (Hartley et al., 2014; Thordarson et al., 1996; Thordarson & Self, 2003). Along with lava effusion and gas emissions, basaltic fissure eruptions may also include explosive phases, producing extensive tephra fall as an additional hazard. In Iceland, for instance, five out of 13 large basaltic fissure eruptions in historical time are associated with widespread tephra layers (e.g., Thordarson & Larsen, 2007). At Laki, eruption plumes reaching maximum heights of 6–13 km produced a tephra blanket of 0.76 km³ in volume (0.4 km³ dense rock equivalent — DRE) (Thordarson & Self, 1993). The explosive phases of basaltic fissure eruptions may span Hawaiian, Strombolian, violent Strombolian and even Plinian eruption styles (Thordarson & Larsen, 2007; Valentine & Gregg, 2008; Walker et al., 1984), but have received comparatively little attention, perhaps because they commonly represent a small volumetric fraction of the eruptive products. Yet, the intensity of these explosive phases control tephra fall hazards and, in part, the climate consequences of a given eruption, because climate-impacting volcanic gases have a much longer atmospheric residence time if injected above the tropopause by tall plumes (e.g., Robock, 2000). A better understanding of explosive activity associated with basaltic fissure eruptions also has important implications for extrapolation to much larger flood basalt eruptions (e.g., Brown et al., 2014; Glaze et al., 2017; Self et al., 2006).

The 1730–1736 CE Timanfaya eruption, on the island of Lanzarote in the Canary Islands, ranks second to Laki among the largest basaltic fissure eruptions of the last millennium globally. This long-duration event (2055 days) produced a complex lava flow field covering 146 km² and at least 2.2–3.7 km³ in volume, destroying 26 villages and forcing the exodus of much of the island's inhabitants (Carracedo et al., 1990, 1992; Carracedo & Rodríguez Badiola, 1991; Longpré & Felpeto, 2021). Timanfaya lavas are characterized by their high MgO content, up to ~17 wt.%, and a temporal-compositional trend from early basanites to late tholeiites (Carracedo et al., 1990, 1992), which attracted substantial attention (Gómez-Ulla et al., 2017, 2018; Lundstrom et al., 2003; Reiners, 2002; Sigmarsson et al., 1998; Thomas et al., 1999). The eruption also produced significant explosive activity, as attested by historical records (Carracedo, 2014; Longpré & Felpeto, 2021; Romero, 2003). However, besides work focusing on post-eruptive sedimentary processes (Criado et al., 2013), the resulting tephra blanket, the most conspicuous part of which forms La Geria, a wine-producing valley (Troll et al., 2017), has not yet been studied in detail.

In this paper, we report the results of fieldwork and geochemical analyses of tephra deposits of the Timanfaya eruption to better constrain its dynamics and style over time. After summarizing relevant background information for context, we document the wide dispersal of

tephra and, based on the distinct chemical fingerprints of the eruptive phases, correlate the distal tephra blanket to its source vents. The results indicate that explosive activity was largely restricted to the initial phase of the eruption and also allow constraining the eruption volume and height of the eruption column. Finally, we draw comparisons with other basaltic eruptions and discuss broader volcanological and environmental implications.

BACKGROUND

Geologic context

The Canary Islands are intraplate volcanic edifices located off the coast of Morocco in the eastern Atlantic Ocean and built on Jurassic oceanic crust (Schmincke et al., 1998). The age of the oldest subaerial volcanic rocks on the seven main islands shows a broad and discontinuous east–west progression, from 20 Ma at Fuerteventura to 1.1 Ma at El Hierro (e.g., van den Bogaard, 2013; Zaczek et al., 2015, and references therein). Lanzarote is the easternmost island of the archipelago (Fig. 1) and comprises two shield complexes — Famara (10.2 to 3.8 Ma) in the north and Los Ajaches (15.5 to 12.3 Ma) in the south (Coello et al., 1992; Perez-Torrado et al., 2023). After an apparent hiatus of 1–2 million years, during which extensive erosion blunted Lanzarote’s topography, rejuvenated volcanism in the Pleistocene produced multiple fissure eruptions, forming northeast–southwest alignments of cinder and tuff cones. La Quemada, Corona, and Los Helechos volcanoes, located in the northeastern part of the island and dated at $\sim 21 \pm 6.5$ ka, may represent the youngest prehistoric eruption on the island (Carracedo et al., 2003). Of the 14 historical eruptions in the Canary Islands since 1500 CE, including the 2021 Cumbre Vieja eruption on La Palma, two took place on Lanzarote, in 1730–1736 and 1824 (Longpré & Felpeto, 2021).

The Timanfaya eruption

Previous work summarized herein (see Longpré & Felpeto, 2021 for details) provides important context on the chronological development of the Timanfaya eruption and the compositional evolution of erupted lavas. Carracedo and Rodríguez Badiola (1991) and Carracedo et al. (1990, 1992) used geologic mapping, analysis of historical sources, and bulk lava compositions to reconstruct the eruption, which was divided into five phases involving ten principal emission centers. Figure 1 shows the location of these main vents and their respective lava flows, as well as a summary eruption chronology, based on these works, whereas Figure 2a,b illustrates the temporal-compositional evolution of erupted lavas using published data for which samples were tied to specific eruptive episodes (Carracedo et al., 1990; Gómez-Ulla et al., 2017; Thomas et al., 1999).

The initial phase of the eruption built three successive cinder cones — Caldera de los Cuervos (1–19 September 1730), Caldera de Santa Catalina (10–31 October 1730) and Pico Partido (10 October 1730 to January 1731) — and a large lava flow field reaching the northwest coast. These flows buried several villages and historical sources also clearly indicate that these early eruptive episodes involved considerable explosive activity. Thick lapilli and ash accumulations damaged roofs and spoiled farmland (Carracedo, 2014; Longpré & Felpeto, 2021; Romero, 2003). Eruptive products at Caldera de los Cuervos are basanites characterized by an abundance of peridotite xenoliths, extremely high MgO (14.1–16.8 wt.%) contents and

high incompatible element concentrations, such as potassium (1.5 wt.%) (Fig. 2a,b). Lavas of Pico Partido and Caldera de Santa Catalina also contain peridotite xenoliths and are mostly alkali basalts; samples generally show high MgO (7.8–13.5 wt.%) and incompatible element concentrations (0.6–1.3 wt.% K₂O), though values are lower than at Caldera de los Cuervos.

Following an apparent hiatus of a few weeks, the second phase of the eruption took place in a least four distinct episodes between March and July 1731, at Montañas del Señalo, located just to the south of Pico Partido. Flows emitted from Montañas del Señalo stretched north near to the large prehistoric tuff cone of Caldera Blanca and southwest towards the towns of Uga and Yaiza. These lavas are xenolith-poor and straddle the compositional divide between alkali and tholeiitic basalt. Their MgO and K₂O contents range from 9.0 to 10.3 wt.% and 0.6–0.8 wt.%, respectively.

Phase III of the eruption began at the end of June 1731 as the activity shifted at least 12 km to the west, initially below sea level and then onshore at the small Volcán El Quemado, which is located ~1 km from the coast and produced a minor alkali basalt lava flow (10.7–11.4 wt.% MgO, 0.7–0.9 wt.% K₂O). The focus of the activity subsequently migrated to the east, forming Montaña Rajada and then Calderas Quemadas, a group of four closely-spaced cinder cones. Lavas from these vents comprise the westernmost expanses of the lava flow field, including along the coastline near to the town of El Golfo. They are alkali to tholeiitic basalts (8.9–11.0 wt.% MgO, 0.6–0.9 wt.% K₂O), with the exception of one sample reported by Thomas et al. (1999) and assigned to Montaña Rajada that is similar to Caldera de los Cuervos lavas.

At this point, the strong impact of the eruption on the island's infrastructure and farmland led to massive exodus of the inhabitants, and as a result contemporary information becomes very scant (Fig. 1b). Based on mapping (Carracedo & Rodríguez Badiola, 1991), the fourth phase of the eruption, beginning in early 1732 and possibly persisting until early 1736, is inferred to have focused at Montañas del Fuego, a large and complex cluster of overlapping cinder cones. Abundant lavas from Montañas del Fuego flowed towards the northwest and southwest, comprising much of the Timanfaya National Park. These lavas are alkali to tholeiitic basalt, with 7.9–11.2 wt.% MgO and 0.6–0.9 wt.% K₂O, except one sample from Thomas et al. (1999) which is a high-MgO basanite.

The fifth and final eruptive phase took place at Montaña de Las Nueces and Montaña Colorada, 5 km east of Montañas del Fuego, but the timing of its onset is uncertain. It was originally deduced that activity at Montaña de las Nueces had occurred from mid-March to early April 1736, producing a large pāhoehoe lava flow that reached the coast near the town of Arrecife to the east (Carracedo et al., 1992; Solana et al., 2004). However, a reassessment of historical archives by Pallarés Padilla (2007) suggests that lava flows emitted from this vent already threatened the town's port by February 1733. If so, Phase V would have begun at least three years earlier than formerly thought. The final emission center of the Timanfaya eruption is Montaña Colorada, which may have been active for only two weeks ending on 16 April 1736. This cone emitted lavas that flowed north, falling just short of reaching the coast, and produced a significant lapilli field on its south flank. Phase V lavas are mostly tholeiitic basalts, showing among the lowest MgO (8.3–11.5 wt.%) and incompatible trace element concentrations (0.6–0.7 wt.% K₂O) of the entire eruptive sequence (Fig. 2a,b). While Montaña de las Nueces lavas are xenolith-poor, Montaña Colorada lavas feature abundant peridotite and silicic xenoliths of metasedimentary origin (Aparicio et al., 2006).

Occurring nearly a century after the Timanfaya eruption, the 1824 eruption was much smaller and shorter in duration (spanning 87 days). It formed three cinder cones, Volcán de Tao, Volcán Nuevo del Fuego, and Volcán de Tinguatón, which are aligned ENE–WSW and spaced by a total of 14 km, and small lava flow fields mostly atop 1730–1736 lavas (Fig. 1) (Longpré & Felpeto, 2021; Romero, 2003). The 1824 lavas are high-MgO basanites, similar in composition to samples from Caldera de los Cuervos and Pico Partido (Fig. 2a,b).

METHODS

Tephrostratigraphy and sampling

The stratigraphy of Timanfaya tephra was documented at 32 localities across Lanzarote (Figs. 3, 4, Table S1). Following a modified grid system, we generally selected sites that were ≥ 10 m away from lava flows on terrain as flat as possible to minimize syn- and post-emplacment deposit reworking effects (e.g., Brown et al., 2015) and that showed no to minimal evidence of anthropogenic disturbance. At each locality, we dug trenches until reaching the underlying orange paleosol. Graphic logs (Fig. 3) were constructed for each site, recording the thickness, componentry, grain size and mineralogy of individual tephra beds, using the terminology and classification scheme of White and Houghton (2006).

Samples were taken at high stratigraphic resolution, from each individual bed identified and deemed in situ (from the lack of evidence of reworking, e.g., cross-bedding) within each trench. At some locations, the bottom and top of particularly thick beds were sampled. We refer to samples collected from trenches, which are all located ≥ 750 m away from the eruptive fissure, as *distal tephtras*, whereas *vent tephtras* correspond to samples collected directly from the flanks of the main cinder cones, thus representing the late stage of individual eruptive episodes.

Density measurements

The density of tephra deposits was estimated in the laboratory. Individual representative lapilli — two from vent tephtras, three from distal tephtras — were weighed in air, subsequently sealed in Parafilm (e.g., Houghton & Wilson, 1989) and submerged in water to obtain their volume by displacement. We assumed that the Parafilm added negligible volume.

The density of lava blocks was measured directly in the field using Archimedes' principle and the methodology of Kueppers et al. (2005). To obtain a representative lava density distribution, we selected blocks of 'a'a' flow tops and cores as well as of pahoehoe flows that averaged 20–40 cm length on any given side. The average bulk lava flow density was then determined using the estimated proportions of flow typologies, as detailed in the [Supplementary Methods and Table S2](#).

X-ray fluorescence

The major and selected trace element composition of bulk rock samples of a set of 15 vent tephtras and ten distal tephtras was analyzed by x-ray fluorescence (XRF) on a Thermo ARL Advant'XP+ XRF sequential spectrometer at Washington State University, based on established protocols (Johnson et al., 1999). Analyses of duplicate samples and of an in-house

standard (COS-M-50; Longpré et al., 2014) were used to confirm the high precision and accuracy of the data (see [Table S3](#) for details).

Electron probe microanalysis

The major and volatile (S, Cl) element concentrations in matrix glasses of 15 vent and 74 distal tephras were measured with a JEOL 8900 electron microprobe at McGill University, using a 15 kV accelerating voltage, 10 nA current, and 15 μm beam size. Sodium was analyzed first to minimize loss by volatilization. Peak/background counting times were 20/10 s for all elements, except Cl (60/30 s) and S (120/60 s). The instrument was calibrated using synthetic and natural standards, including the Makahoupi basaltic glass standard USNM 113498 A-99 (Jarosewich, 2002) for Si, Ti, Mg, Fe, Al, Ca, and Na and KE-12 obsidian glass (Devine et al., 1995a) for K. Data quality was monitored by replicate analyses of VG-2 (USNM 111240-52) (Jarosewich, 2002) and P1326-2 (Stix et al., 1995) basaltic glasses during our analytical session ([Table S3](#)).

Inductively coupled plasma mass spectrometry

Bulk rock samples of four selected vent tephras were analyzed for trace element concentrations by inductively coupled plasma mass spectrometry (ICP-MS) on an Agilent 7700 quadrupole instrument using a routine method at the GeoAnalytical Lab of Washington State University, which has a long-term relative precision (1σ) better than 5% for rare earth elements and 10% for other elements (Knaack et al., 1994). As for XRF, one of our samples was run in duplicate, showing reproducibility better than 3% relative for all elements, and standard COS-M-50 was also run to check accuracy, with data agreeing with preferred values within 10% relative ([Table S3](#)).

Matrix glasses of 15 vent and 58 distal tephras were analyzed by laser ablation ICP-MS for trace element abundances at Lamont-Doherty Earth Observatory of Columbia University, using an ESI New Wave UP 193 FX excimer laser coupled to a VG ExCell quadrupole mass spectrometer. Samples were ablated in an Ar-He mixture at a flow rate of $\sim 0.6 \text{ mL min}^{-1}$ and 1.6 mL min^{-1} , respectively, using the laser in spot-drill mode at 10 Hz and 90% power, giving a mean energy density of 11.3 J cm^{-2} and irradiance of 2.26 GW cm^{-2} . Spectra were collected by peak-hopping; dwell times were 10 ms for all analytes, of which ^{43}Ca was used for normalization. Beam sizes of 50 and 75 μm were used for unknowns and standard glasses (BCR-2G, BIR-1G, and BHVO-2G), respectively. Counting times were 60 s on background and 60 s on peak. Calibration curves defined by the standards were linear ($R^2 \geq 0.99$). The high precision and accuracy of the data were confirmed by replicate analyses in-house standard P1326-2 ([Table S3](#)). Data reduction was completed using the LasyBoy macro (v. 3.77f; J. Sparks, Boston University), and GeoReM preferred values (Jochum & Nohl, 2008) for the compositions of USGS glass standards.

RESULTS AND DISCUSSION

Tephra componentry and dispersal

Cinder cones associated with the Timanfaya eruption are built by both agglutinate spatter and loose pyroclasts (see also Kervyn et al., 2012), which are dominantly gray to black,

glassy and scoriaceous lapilli and ash. Tephra at Caldera de los Cuervos is characterized by a blueish, pseudo-iridescent sheen, whereas that at Montaña Colorada is distinct, consisting in part of a light golden brown, frothy scoria. Clasts are generally olivine-phyric, with individual olivine crystals typically up to 1 mm in size. Larger crystal clots, frequently ≥ 1 cm across, are common and likely represent disaggregated peridotite xenoliths. Such xenoliths attain dimensions of ~ 30 cm in the crater walls of Caldera de los Cuervos and occur as brick-sized bombs on the flanks of Pico Partido.

At locations away from the eruptive fissure, fresh tephra occurs immediately above a conspicuous orange paleosol comprising volcanoclastic and aeolian sediments that formed over ~ 40 ky (Criado et al., 2013; Jahn & Stahr, 1996; von Suchodoletz et al., 2008). This laterally extensive tephra almost certainly derives from the Timanfaya eruption, consistent with radiocarbon ages bracketing it between the 14th and 19th century (Criado et al., 2013). [Figure 3](#) shows selected stratigraphic sections through this distal tephra from representative localities across Lanzarote. The deposit chiefly comprises gray to black, glassy ash- to lapilli-sized clasts. At several localities (e.g., LZ-4), we identified horizons rich in Pele's hair, as observed in the Laki tephra (Thordarson & Self, 1993), suggesting rapid tephra accumulation rates allowing preservation of these delicate fragments. Peridotite lithics as well as white to gray pumice-like clasts are also occasionally found, the latter resembling "xeno-pumices" commonly co-erupted with mafic magma in the Canaries and thought to represent melted silicic sediments (e.g., Aparicio et al., 2006; Carracedo et al., 2022; Troll et al., 2012).

The total thickness of the tephra blanket at the studied sites is shown in [Figure 4a](#). These data confirm the wide dispersal of the Timanfaya pyroclasts, consistent with the data of Criado et al. (2013) as well as with historical sources reporting ashfall across much of Lanzarote and as far as neighboring Fuerteventura (Carracedo, 2014; Romero, 2003). For instance, at Caldera de Gaida ~ 5 km south of the fissure (locality LZ-4), the tephra exceeds 1 m thickness. At our most distal location (LZ-3) — at an incised hillside near Guatiza ~ 20 km northeast of Montaña Colorada, corresponding to locality 5 of Criado et al. (2013) — the fine tephra layer is 10 cm thick. Tephra thickness is generally greater south of the eruptive fissure, reaching an observed maximum of 1.8 m, likely reflecting dominant northerly winds ([Fig. 4b](#)). We note that tephra dispersal by northerly winds also appears to commonly affect the morphology of cinder and tuff cones on Lanzarote, including Caldera de los Cuervos, with southern crater rims typically showing higher elevations than northern crater rims (Kervyn et al., 2012).

The Timanfaya tephra displays internal stratification most often delineated by abrupt changes in grain size ([Fig. 3](#)). Beds at the base of the sections are often the coarsest, with maximum clast size up to 5 cm at trench LZ-24, and thickest (~ 10 cm) ([Figs. 3, 4](#)); they also commonly exhibit a pseudo-iridescent sheen, reminiscent of Caldera de los Cuervos vent tephra. Grain size and bed thickness decrease, while sorting generally increases up-section. Tephra at most trenches is moderately well sorted, with a broad positive relationship between trench distance from the fissure and sorting. Minor lithological variation occurs in the uppermost strata deemed in situ of some trenches, in any of three ways: (1) pyroclasts may culminate in a thin (a few cm) layer of light brown, frothy scoria similar in appearance to that found on the summit of Montaña Colorada ([Fig. 3c](#)); (2) small (≤ 1 cm) light-colored lithic clasts resembling metasedimentary xenoliths from Montaña Colorada may increase in abundance; and (3) at three localities, deposits include a thin layer of accretionary lapilli. We also identified two

horizons containing plant roots (Fig. 3), ~10 cm below the top of each respective section (LZ-14 and LZ-15, which both exceed 1 m thickness). We speculate that these roots may mark the interface between Timanfaya tephras and locally preserved, thin deposits from the 1824 eruption.

Tephra composition and distal tephra–source vent correlation

All geochemical data on our Timanfaya samples are reported in Table S4. The bulk rock composition of vent tephras shows ranges of 43.0–50.9 wt.% SiO₂ and 4.7–3.3 wt.% total alkalis (Fig. 2c), closely replicating the early basanite to late tholeiite trend previously established based on lava samples (Fig. 2a) (Carracedo et al., 1990). Tephras from Phase I vents are highly enriched in incompatible trace element concentrations, also in line with published data (Fig. 5a). In addition, trace element ratios, such as Zr/Nb, of vent samples correlate well with those of corresponding lava samples, confirming the lava–source vent associations defined by Carracedo et al. (1990) (Fig. 2d).

The matrix glasses of vent tephras (43.4–53.0 wt.% SiO₂, 6.4–3.6 wt.% total alkalis) are broadly similar to their respective bulk rocks, also shifting from basanitic to tholeiitic compositions over the eruption sequence (Fig. 2e). Glasses show much lower MgO contents (5.0–6.2 wt% MgO, vs. 9.4–14.0 wt% in the bulk rocks, Fig. 2f), however, reflecting the olivine-rich crystal cargo of the bulk rocks (see also Gómez-Ulla et al., 2017). Importantly, as for bulk rocks, incompatible element concentrations vary substantially in glasses from different eruption phases, with samples from Caldera de los Cuervos, Pico Partido and Caldera de Santa Catalina consistently displaying the most enriched compositions (Fig. 5b). Glasses from these earliest eruptive episodes also exhibit negative high field strength element (HFSE, e.g., for Zr and Hf) anomalies, which are not observed in samples from subsequent eruptive phases. Ratios of highly incompatible to moderately incompatible elements provide additional useful proxies for the degree of enrichment. For example, we find that Nb/Y ratios are up to a factor of two higher in Phase I basanitic tephras relative to Phase V tholeiitic tephras (Fig. 6b). Finally, vent tephra glasses are also characterized by decreasing chlorine concentrations over the eruptive sequence, from 900 ppm at Caldera de los Cuervos to 300 ppm at Montaña Colorada (Fig. 7a). Chlorine is little affected by syn-eruptive degassing in Canary Island magmas (Longpré et al., 2017), and these Cl abundances at Timanfaya generally exceed Cl concentrations in melt inclusions from Laki (200–310 ppm, Thordarson et al., 1996). Sulfur concentrations, on the other hand, are generally low to below detection limit of our EPMA setup (i.e., <140 ppm, Table S4), due to effective syn-eruptive degassing.

For distal tephras, limited bulk rock data are consistent with vent tephra compositions, with SiO₂ contents increasing from 43.4 to 48.0 wt.% as total alkalis decrease from 4.5 to 3.6 wt.% (Fig. 2c). However, more abundant EPMA and LA-ICP-MS data on matrix glasses allow a fuller characterization of distal tephra compositions and comparison with vent tephras. We find that, while distal tephra glasses overall span a slightly wider compositional range than those of vent samples, most are characterized by low SiO₂, high incompatible element concentrations, high chlorine and negative HFSE anomalies (Figs. 2e, 5b, 6, 7). These characteristics strongly resemble the composition of Phase I vent tephras, suggesting most distal tephras were sourced from Caldera de los Cuervos, Pico Partido and Caldera de Santa Catalina.

To test and quantify this further, we assigned each distal tephra sample to its likeliest source vent by exploiting the distinct signatures of eruptive episodes in P₂O₅–SiO₂ and Nb/Y–SiO₂ spaces (Fig. 6). In this approach, we used the Euclidean distance formula to solve for the distance between each distal sample and all the vent samples — the shortest distance obtained then ties each distal tephra to its source vent. The resulting distal tephra–source vent associations, which are very similar for P₂O₅–SiO₂ and Nb/Y–SiO₂, are listed in Table S5 and allow reconstructing the stratigraphic sequence at each of our trench sites (Fig. 3).

We find that this geochemistry-based stratigraphic reconstruction is broadly consistent with the eruption chronology of Carracedo et al. (1990, 1992). For example, at trench LZ-28, we observe tephra assigned to Pico Partido overlying tephra sourced from Caldera de Santa Catalina, in agreement with historical records indicating that activity at Pico Partido persisted longer than it did at Caldera de Santa Catalina.

Most importantly, we find that 33–38% of distal tephtras are correlated to Caldera de los Cuervos, 10–12% to Pico Partico and 38–41% to Caldera de Santa Catalina, with the remainder mostly matched to Montañas del Fuego (8–9%) — transitional to tholeiitic tephtra compositions from other episodes appear largely missing from our distal sites. This confirms that the bulk of the tephtra blanket associated with the Timanfaya eruption was emplaced between September 1730 and January 1731, consistent with historical records and the preliminary analysis of Criado et al. (2013). In other words, substantial explosive activity was largely restricted to the initial stages of the eruption, involving basanite to alkali basalt magma.

Eruption volume and dynamics

In this section, we begin by discussing constraints on the volume of Timanfaya lavas and then use our data to derive estimates of tephtra volume as well as peak eruption column height.

Lava volume

As reviewed by Longpré and Felpeto (2021), published estimates of lava flow volume for the Timanfaya eruption range from 1 to 5 km³, with a mean of 2.5 ± 1.4 km³. Timanfaya lavas reach thicknesses on the order of 50 m on the west coast of Lanzarote, but are much thinner in other parts of the flow field, and mean lava thickness is poorly known. Assuming mean thicknesses similar to well-constrained Icelandic lava flow fields (~15–25 m, Pedersen et al., 2017; Thordarson & Self, 1993), Longpré and Felpeto (2021) estimated a lava flow volume of 2.2–3.7 km³, based on an area of 146 km². In addition, these authors devised an empirical relationship based on area–volume data of other basaltic eruptions which yielded 4.3 km³ for Timanfaya. While plausible, these estimates remain rough. More robust determination of lava volume at Timanfaya may be obtained by near-surface geophysical surveys onland (e.g., ground penetrating radar, Gómez-Ortiz et al., 2014) and high-resolution mapping of the submarine extent of the flow field along large portions of the coastline (e.g., Soule et al., 2019). Our field measurements of lava block density ($n = 28$), which yield a weighted mean of 2,120 kg/m³ (Table S2), can be used to better constrain DRE volumes from bulk lava volumes that include pore space; e.g., the preferred bulk volume range of 2.2–3.7 km³ above yields 1.7–2.8 km³ DRE, assuming a magma density of 2,800 kg/m³.

Tephtra volume

Based on tephtra thickness data, we used a regularized spline contouring method (Engwell et al., 2015) to construct 5 isopachs — at thicknesses of 10, 20, 40, 80, and 160 cm — in an effort to balance precision against the potential of overfitting the data (Fig. 4a, Supplementary Methods). The total area enclosed within each isopach was calculated using ArcGIS. In Figure 8, tephtra thickness is plotted against the square root of area, which effectively normalizes the deposit to an ideal, concentric form and allows calculating its volume by integrating under the curve (Pyle, 1989). Using AshCalc software (Daggitt et al., 2014), we fitted the isopach data with a single exponential segment, which yields a bulk tephtra blanket

volume of 0.44 km³. Based on density measurements of individual pyroclasts ($n = 5$) yielding $1,260 \pm 240$ kg/m³ (Table S2), this figure may be converted to 0.20 km³ DRE.

We believe our bulk tephra blanket volume to be a relatively robust minimum estimate, as replicate analyses using different methods, i.e., multi-segment exponential thinning and Weibull thinning (Bonadonna & Costa, 2012), agree within ~10% (see Supplementary Methods). However, our data do not allow constraining the 1 cm isopach, which may contain a significant fraction of the deposit (Bonadonna & Costa, 2012). Historical records of ash fall on Fuerteventura (Romero, 2003) at least 30 km away from Phase I vents attest to significant tephra fall beyond our field sites, with some lost to sea. The above figure also excludes the proximal tephra volume contained within the cones. On the basis of idealized cone volume calculations with cone height and cone diameter measured in ArcGIS, we estimate the main ~15 cones constructed over the course of the eruption to sum to ~0.1 km³. In comparison, Kervyn et al. (2012) obtained 0.07 km³ for Timanfaya cones (M. Kervyn, personal communication, 2020). As the density of cone-building agglutinated spatter and lapilli is likely between that of lavas and loose pyroclasts (i.e., in the range 1,260–2,120 kg/m³), we deduce a DRE cone volume between 0.03 and 0.08 km³. Hence the minimum combined proximal and distal tephra volume is 0.51–0.54 km³ (0.23–0.28 km³ DRE).

Eruption column height

The maximum grain size of tephra fall deposits is a function of distance from the vent and the eruption explosivity, and it may be used to estimate eruption column height (e.g., Pyle, 1989) — a parameter that is ill-constrained for historical Canary Island eruptions (Longpré & Felpeto, 2021). However, cinder cone eruptions are commonly pulsatory (e.g., Pioli et al., 2008), and, in the case of the Timanfaya eruption, we infer the tephra blanket to have accumulated over 3–4 months in multiple pulses primarily from three point sources: Caldera de los Cuervos, Pico Partido and Caldera de Santa Catalina. In this context, our approach to constrain maximum eruption column height focuses on the distinctive basal lapilli bed, which is present in several trenches and tied to Caldera de los Cuervos based on componentry and composition (Fig. 3). This bed is interpreted to relate to a particularly vigorous eruption pulse near the eruption's inception, as it is commonly the thickest and coarsest at any given locality.

In Figure 4b, two sets of isopleths are thus shown — one for the full deposit, the other for the basal bed only. Contouring is performed as described for isopachs. The number of data points for the basal bed is restricted (eight), likely causing contouring artifacts. Nevertheless, basic inferences can be made. The east–west extent of the 10 mm isopleth indicates that the explosive activity of Caldera de los Cuervos, from 1 to 19 September 1730, affected an area almost as large as that of the cumulative whole of the Timanfaya eruption. Indeed, 10-mm lapilli reached more than 10 km from the vent. Using a MATLAB implementation (Biass et al., 2015) of the model of Carey and Sparks (1986), we utilized our isopleth data to constrain eruptive plume height above the crater, which is ~320 m above sea level (Longpré & Felpeto, 2021). Based on the 20 mm isopleth and the measured bulk tephra density (1,260 kg/m³, Table S2), we obtain eruption columns reaching 8 km, which is taken as a minimum value as eruption plumes may reach beyond their level of neutral buoyancy (Carey & Sparks, 1986).

Comparison to other explosive basaltic eruptions

To put our findings in a wider context, a comparison of the Timanfaya eruption with other explosive basaltic eruptions is useful. First, we note that the tephra volume produced by the Timanfaya eruption (0.51–0.54 km³) approaches that of the Laki eruption (0.76 km³), despite a much smaller total eruptive volume. In [Figure 8](#), the Timanfaya deposits plot above the 2021 Cumbre Vieja deposits (Bonadonna et al., 2022), but below the long-lasting monogenetic events at El Jorullo (1759–1774) and Parícutin (1943–1952), Mexico (Pioli et al., 2008; Rowland et al., 2009), and large basaltic Plinian eruptions, such as the 1886 Tarawera eruption (Walker et al., 1984), the 122 B.C. Etna eruption (Coltelli et al., 1998) and the late-Pleistocene Fontana Lapilli from the Masaya-Las Sierras volcanic system in Nicaragua (e.g., Costantini et al., 2009).

In terms of plume height, our estimate for Timanfaya compares well with the lower end of values inferred for Laki (6–13 km, Thordarson & Self, 1993) and other explosive basaltic eruptions, such as the 1992 eruption of Cerro Negro (Connor & Connor, 2006). It is however significantly lower than those of the aforementioned basaltic Plinian eruptions, with column heights in the 24–32 km range (Coltelli et al., 1998; Costantini et al., 2009; Walker et al., 1984). Our values also coincide with the highest eruption column heights observed for the 2021 eruption of Cumbre Vieja volcano on La Palma, which produced sustained ash-rich plumes that were most frequently in the 2–4 km height range but reached up to 8.5 km (Bonadonna et al., 2022). This led to widespread and thick tephra accumulation at Cumbre Vieja, reaching thicknesses of ~4 m at an 850-m distance in the main dispersal axis southwest of the vent (Bonadonna et al., 2022; Rodríguez et al., submitted). We envisage the explosive activity during Phase I of the Timanfaya eruption to have been similar to, though of greater volume than, that of the 2021 Cumbre Vieja eruption.

Our results at Timanfaya, together with the work of Di Roberto et al. (2016) on the 1909 Chinyero eruption on Tenerife and recent direct observations at Cumbre Vieja, thus demonstrate the explosive potential of violent Strombolian activity at Canary Island volcanoes and, more broadly, add to a growing body of evidence indicating that cinder cone-producing basaltic eruptions commonly involve significant explosive activity (e.g., Alfano et al., 2019; Bonadonna et al., 2022; Martí et al., 2017; Pioli et al., 2008).

Volcanological and environmental implications

In this final discussion section, we address broader implications of our findings on the Timanfaya eruption pertaining to (1) the style of basaltic fissure eruptions, (2) a potential link between eruptive style and magma composition and (3) possible environmental impacts.

Style and classification of large basaltic fissure eruptions

As highlighted in this work, large basaltic fissure eruptions, such as Timanfaya and Laki, may comprise explosive phases, although they are volumetrically dominated by lava outpourings. As a result, these eruptions are difficult to encapsulate in simple hazards assessment schemes. For example, the Global Volcanism Program (www.volcano.si.edu) database lists a Volcanic Explosivity Index (VEI, Newhall & Self, 1982) of 3 and 4 for Timanfaya and Laki, respectively. Indeed, using estimates of eruption column heights of 8 km for Timanfaya (this work) and 13 km for Laki (Thordarson & Self, 1993), we arrive at corresponding VEI values of 3 and 3–4. However, based on estimates of eruptive volume, a criterion which was deemed more reliable by Newhall and Self (1982), VEI values raise to 5 for Timanfaya

(2.7–4.2 km³ bulk) and 6 for Laki (15.5 km³ bulk). While the VEI was primarily developed to describe the explosive magnitude of eruptions, it has become a basis in a number of approaches to quantifying and communicating volcanic risk (e.g., Brown et al., 2015; Mani et al., 2021; Scandone et al., 2016). In this context, we argue that the higher VEI values based on eruptive volume, which are more in line with magnitude (M) estimates based on erupted mass (Pyle, 2015), better represent of the potential hazards and impacts of such eruptions.

A link between eruptive style and magma composition?

At Kilauea volcano, Hawaii, it has been suggested that eruptive style is partially controlled at the magmatic source, i.e., in a bottom-up fashion, whereby primary melts enriched in incompatible trace elements and volatiles are more prone to erupt explosively (Sides et al., 2014). Our data appear tentatively consistent with such a scenario at Timanfaya, as the most enriched magmas erupted more explosively in Phase I. Similar basanitic magmas from the island of El Hierro are volatile-rich and may contain up to several wt.% CO₂, 3 wt.% H₂O and 0.5 wt.% S prior to degassing (Longpré et al., 2017; Taracsák et al., 2019), and preliminary reports of volatile contents in Timanfaya magmas are consistent with such values (Gómez-Ulla et al., 2019; Sharma et al., 2005). Although analysis of volatile concentrations in melt inclusions is beyond the scope of this study, we can utilize trace elements that partition similarly to specific volatiles during melting and crystallization to obtain first-order estimates of undegassed volatile contents (Longpré et al., 2017; Saal et al., 2002). For this exercise, illustrated in [Figure 7](#), we take Ba and Nb as proxies for CO₂, Ce for H₂O, Dy for S and K for Cl and assume mantle volatile/lithophile elemental ratios of 105 for CO₂/Ba (Michael & Graham, 2015), 505 for CO₂/Nb (Rosenthal et al., 2015), 200 for H₂O/Ce (Michael, 1995; Saal et al., 2002), 370 for S/Dy (McDonough & Sun, 1995) and 0.11 for Cl/K (Palme & O'Neill, 2003). This analysis is consistent with generally high volatile contents (>1.5 wt.% CO₂, >0.8 wt.% H₂O, >1,500 ppm S) in undegassed Timanfaya magmas, but the highest values are predicted for the Caldera de los Cuervos basanite (>3.8 wt.% CO₂, >2.3 wt.% H₂O, >2,300 ppm S). If confirmed by melt inclusion analysis, such high initial volatile contents could represent the driving force for the explosive onset of the eruption, which would be consistent with a causative link between magma composition and eruptive style (Sides et al., 2014). Alternatively, explosive activity during Phase I may be explained by efficient segregation of large amounts of excess gas in the upper part of the plumbing system and ascending dike (Menand & Tait, 2001; Rubin, 1995).

A climate impact for the Timanfaya eruption?

Based on an eruptive volume of 1.9 to 3.1 km³ DRE, a magma density of 2,800 kg/m³, predicted CO₂ and S concentrations of 1.5–5 wt.% and 2,000–3,000 ppm, respectively ([Fig. 7b,c](#)), and assuming 100% syn-eruptive degassing (which is consistent with negligible S concentrations in our matrix glasses), we calculate the Timanfaya eruption could have released 81–431 Tg CO₂ and 11–26 Tg S to the atmosphere. For sulfur, Sharma et al. (2005) arrived at a value near the middle of this range (20 Tg S) based on melt inclusion work. This is about twice the amount released by the 1991 eruption of Mount Pinatubo (e.g., Guo et al., 2004). Given the substantial sulfur yields for the much smaller 2011–2012 El Hierro (1.8–2.9 Tg S, Longpré et al., 2017) and 2021 La Palma (0.6–2.0 Tg S, Hayer et al., 2022) eruptions, such a sizable sulfur output at Timanfaya is perhaps not surprising, but it raises the question of possible climate and

environmental consequences of the eruption. However, ice core evidence for a stratospheric transport of sulfur associated with Timanfaya is ambiguous at best (Fig. 9a). While Hammer et al. (1980) and Zielinski (1995) respectively reported a 1730–1736 acidity peak and a 1731 sulfate anomaly in single Greenland ice cores, more recent multi-core compilations documented Northern Hemisphere anomalies for 1729 (Gao et al., 2008; Sigl et al., 2015) and 1739 (Sigl et al., 2015), but none in the 1730–1736 range that could be associated with Timanfaya. Intriguingly, an analysis of the Global Volcanism Program eruption catalogue yields no obvious candidate for the 1729 sulfate anomaly. The poorly known 1727–1728 Oraefajokull (Iceland) eruption (Forbes et al., 2014), listed as a VEI 4, has been proposed (Zielinski, 1995), but given its proximal location to Greenland and end date around May 1728 it appears too old to have produced the 1729 anomaly. In contrast, the 1739 signal is likely tied to the 1739 VEI 5 eruption of Shikotsu (Tarumai) volcano in Japan (Toohey & Sigl, 2017). Nevertheless, a lack of widespread Timanfaya signal in polar ice cores is consistent with the tropospheric eruption columns indicated by our data.

Yet, other lines of evidence suggest a significant environmental impact of the eruption. For instance, a continental-scale temperature reconstruction for Europe and the Arctic (Fig. 9b) (PAGES 2k Consortium, 2013) shows a marked negative anomaly in the first half of the 1730's. In addition, the Northern Hemisphere tree ring density network of Briffa et al. (1998) indicates a summer temperature anomaly of -0.25 °C for 1731, comparable to -0.27 °C for 1783 (Laki) and -0.30 °C for 1992 (Pinatubo), and bristlecone pines from the western USA also show a frost ring for 1732 (Salzer & Hughes, 2007). In comparison, however, the Northern Hemisphere composite (N-Tree) of Sigl et al. (2015) displays little to no anomaly associated with Timanfaya (Fig. 9b). For the tropics, a multi-proxy reconstruction of annual sea surface temperatures (Fig. 9c) (D'Arrigo et al., 2009) yields an anomaly of -0.90 °C for 1731, the coldest value of the past four centuries. In this dataset, 1730 also ranks 12th (-0.69 °C), whereas cooling associated with Laki appears minor in the tropics (-0.30 °C). Finally, the environmental effects of the Timanfaya eruption may also be recorded by iron anomalies found in tree rings from the Pyrenees (Hevia et al., 2018) and in historical accounts of dry fog occurrence in Italy (Camuffo & Enzi, 1995). From these integrated observations, we conclude that the Timanfaya eruption likely had hemispheric climate and environmental repercussions. Interestingly, as a side note, this analysis also indicates a marked climate impact for the 1739 Tarumai eruption and, to a lesser extent, for the 1766 Hekla eruption (Fig. 9a,b).

CONCLUSIONS

The main findings of our investigation of tephra deposits sourced from the 1730–1736 CE Timanfaya eruption may be summarized as follows:

- (1) Stratigraphic sections show that tephra produced by the eruption was widely dispersed across most of Lanzarote and formed a blanket of ~ 0.44 km³ in bulk volume (0.20 km³ DRE). The total tephra volume, including the cones, is 0.51–0.54 km³ (0.23–0.28 km³ DRE).
- (2) Nearly all distal tephtras show basanite–alkali basalt compositions highly enriched in incompatible trace elements that only match tephra originating from the first three vents: Caldera de los Cuervos, Pico Partido and Caldera de Santa Catalina. Thus, the most

violent explosive activity was restricted to the initial phase of the eruption, but particularly its first few weeks, followed by prolonged, dominantly effusive activity.

- (3) Isopeleth data from a particularly thick and coarse basal bed tied to Caldera de los Cuervos indicates that the highest eruption columns rose to at least 8 km.
- (4) Given their sizable hazards and potential environmental impacts, we propose that large basaltic fissure eruptions are better represented by VEI values based on eruptive volume, rather than plume height.
- (5) Eruptive style is broadly correlated with magma composition at Timanfaya, and trace element proxies indicate that explosively-erupted basanite–alkali basalt magmas were richer in volatiles compared to effusively-erupted tholeiites, but a causative link remains to be tested.
- (6) We estimate that the Timanfaya eruption released 11–26 Tg of sulfur (and 81–431 Tg CO₂) to the atmosphere. Whether some of this sulfur reached Greenland via stratospheric transport is equivocal, but several proxy records suggest the eruption had a hemispheric environmental impact.
- (7) Our results add to a growing body of evidence that mafic Canary Island volcanism, and basaltic fissure eruptions in general, frequently involve vigorous explosive activity.

ACKNOWLEDGEMENTS

This work results from the master's thesis research of J.K.M. at Queens College, City University of New York. We are grateful to the Cabildo de Lanzarote for providing permits to conduct fieldwork and sampling within the Parque Nacional de Timanfaya and the Parque de los Volcanes. We thank Patrick Beaudry, Elena Mateo and Ana Garmendia who helped with fieldwork and Alia Lesnek who helped generating the DEM basemap. Lang Shi and Louise Bolge provided invaluable support during EPMA and LA-ICP-MS analysis, respectively. This work benefitted from discussions with Don Swanson, Ray Cas, Gert-Jan Peeters, William Moreland and Tim Clements. Jeffrey Marsh and Philipp Ruprecht provided useful comments on an earlier version of this manuscript. This work was supported through a Graduate Student Research Grant #11085-15 from the Geological Society of America to J.K.M. and through National Science Foundation Award # 1944723 and a Queens College Research Foundation grant, including partial support from the Paula and Jeffrey Gural Endowed Professorship in Geology, to M.-A.L.

REFERENCES

- Alfano, F., Ort, M. H., Pioli, L., Self, S., Hanson, S. L., Roggensack, K., Allison, C. M., Amos, R., & Clarke, A. B. (2019). Subplinian monogenetic basaltic eruption of Sunset Crater, Arizona, USA. *GSA Bulletin*, 131(3–4), 661–674. <https://doi.org/10.1130/B31905.1>
- Aparicio, A., Bustillo, M. A., Garcia, R., & Araña, V. (2006). Metasedimentary xenoliths in the lavas of the Timanfaya eruption (1730–1736, Lanzarote, Canary Islands): Metamorphism and contamination processes. *Geological Magazine*, 143(2), 181–193. <https://doi.org/10.1017/S0016756806001713>
- Biass, S., Bagheri, G., & Bonadonna, C. (2015). A Matlab implementation of the Carey and Sparks (1986) model to estimate plume height and wind speed from isopleth maps. *Department of Earth Sciences, University of Geneva, Switzerland*. <https://vhub.org/resources/3922>
- Bonadonna, C., & Costa, A. (2012). Estimating the volume of tephra deposits: A new simple strategy. *Geology*, 40(5), 415–418. <https://doi.org/10.1130/G32769.1>
- Bonadonna, C., Pistolesi, M., Biass, S., Voloschina, M., Romero, J., Coppola, D., Folch, A., D'Auria, L., Martin-Lorenzo, A., & Dominguez, L. (2022). Physical characterization of long-lasting hybrid eruptions: The 2021 Tajogaite eruption of Cumbre Vieja (La Palma, Canary Islands). *Journal of Geophysical Research: Solid Earth*, 127(11), e2022JB025302. <https://doi.org/10.1029/2022JB025302>
- Briffa, K. R., Jones, P. D., Schweingruber, F. H., & Osborn, T. J. (1998). Influence of volcanic eruptions on Northern Hemisphere summer temperature over the past 600 years. *Nature*, 393(6684), 450–455. <https://doi.org/10.1038/30943>
- Brown, R. J., Blake, S., Thordarson, T., & Self, S. (2014). Pyroclastic edifices record vigorous lava fountains during the emplacement of a flood basalt flow field, Roza Member, Columbia River Basalt Province, USA. *GSA Bulletin*, 126(7–8), 875–891. <https://doi.org/10.1130/B30857.1>
- Brown, R. J., Thordarson, T., Self, S., & Blake, S. (2015). Disruption of tephra fall deposits caused by lava flows during basaltic eruptions. *Bulletin of Volcanology*, 77, 1–15. <https://doi.org/10.1007/s00445-015-0974-3>
- Brown, S. K., Auker, M. R., & Sparks, R. S. J. (2015). Populations around Holocene volcanoes and development of a Population Exposure Index. In S. C. Loughlin, R. S. J. Sparks, S. K. Brown, S. F. Jenkins, & C. Vye-Brown (Eds.), *Global Volcanic Hazards and Risk* (pp. 223–232). Cambridge University Press.
- Camuffo, D., & Enzi, S. (1995). Impact of the clouds of volcanic aerosols in Italy during the last 7 centuries. *Natural Hazards*, 11, 135–161. <https://doi.org/10.1007/BF00634530>
- Carey, S., & Sparks, R. S. J. (1986). Quantitative models of the fallout and dispersal of tephra from volcanic eruption columns. *Bulletin of Volcanology*, 48, 109–125. <https://doi.org/10.1007/BF01046546>
- Carracedo, J. (2014). The 1730–1736 Eruption of Lanzarote, Canary Islands. In F. Gutiérrez & M. Gutiérrez (Eds.), *Landscapes and Landforms of Spain* (pp. 273–288). Springer Netherlands. https://doi.org/10.1007/978-94-017-8628-7_23
- Carracedo, J. C., & Rodríguez Badiola, E. (1991). *Lanzarote. La erupción volcánica de 1730*. Cabildo Insular de Lanzarote, Servicios de Publicaciones.
- Carracedo, J. C., Rodríguez Badiola, E., & Soler, V. (1990). Aspectos volcanológicos y estructurales, evolución petrológica e implicaciones en riesgo volcánico de la erupción de 1730 en Lanzarote, Islas Canarias. *Estudios Geológicos*, 46(1–2), 25–55. <https://doi.org/10.3989/egeol.90461-2436>
- Carracedo, J. C., Rodríguez Badiola, E., & Soler, V. (1992). The 1730-1736 eruption of Lanzarote, Canary Islands: A long, high-magnitude basaltic fissure eruption. *Journal of Volcanology and Geothermal Research*, 53(1–4), 239–250. [https://doi.org/10.1016/0377-0273\(92\)90084-Q](https://doi.org/10.1016/0377-0273(92)90084-Q)

- Carracedo, J. C., Singer, B., Jicha, B., Guillou, H., Rodríguez Badiola, E., Meco, J., Pérez Torrado, F. J., Gimeno, D., Socorro, J. S., & Láinez, A. (2003). La erupción y el tubo volcánico del Volcán Corona (Lanzarote, Islas Canarias). *Estudios Geológicos*, 59(5–6), 277–302. <http://hdl.handle.net/10261/2329>
- Carracedo, J. C., Troll, V. R., Day, J. M., Geiger, H., Aulinas, M., Soler, V., Deegan, F. M., Perez-Torrado, F. J., Gisbert, G., & Gazel, E. (2022). The 2021 eruption of the Cumbre Vieja volcanic ridge on La Palma, Canary Islands. *Geology Today*, 38(3), 94–107. <https://doi.org/10.1111/gto.12388>
- Coello, J., Cantagrel, J. M., Hernan, F., Fuster, J. M., Ibarrola, E., Ancochea, E., Casquet, C., Jamond, C., Diaz De Teran, J. R., & Cendrero, A. (1992). Evolution of the eastern volcanic ridge of the Canary Islands based on new K-Ar data. *Journal of Volcanology and Geothermal Research*, 53(1–4), 251–274. [https://doi.org/10.1016/0377-0273\(92\)90085-R](https://doi.org/10.1016/0377-0273(92)90085-R)
- Coltelli, M., Del Carlo, P., & Vezzoli, L. (1998). Discovery of a Plinian basaltic eruption of Roman age at Etna volcano, Italy. *Geology*, 26(12), 1095–1098. [https://doi.org/10.1130/0091-7613\(1998\)026<1095:DOAPBE>2.3.CO;2](https://doi.org/10.1130/0091-7613(1998)026<1095:DOAPBE>2.3.CO;2)
- Connor, L. J., & Connor, C. B. (2006). Inversion is the key to dispersion: Understanding eruption dynamics by inverting tephra fallout. In H. M. Mader, S. G. Coles, C. B. Connor, & L. J. Connor (Eds.), *Statistics in Volcanology* (Vol. 1, p. 0). Geological Society of London. <https://doi.org/10.1144/IAVCEI001.18>
- Costantini, L., Bonadonna, C., Houghton, B., & Wehrmann, H. (2009). New physical characterization of the Fontana Lapilli basaltic Plinian eruption, Nicaragua. *Bulletin of Volcanology*, 71(3), 337–355. <https://doi.org/10.1007/s00445-008-0227-9>
- Criado, C., Dorta, P., Bethencourt, J., Navarro, J., Romero, C., & García, C. (2013). Evidence of historic infilling of valleys in Lanzarote after the Timanfaya eruption (AD 1730–1736, Canary Islands, Spain). *The Holocene*, 23(12), 1786–1796. <https://doi.org/10.1177/0959683613505342>
- Daggitt, M. L., Mather, T. A., Pyle, D. M., & Page, S. (2014). AshCalc—a new tool for the comparison of the exponential, power-law and Weibull models of tephra deposition. *Journal of Applied Volcanology*, 3, 1–8. <https://doi.org/10.1186/2191-5040-3-7>
- D'Arrigo, R., Wilson, R., & Tudhope, A. (2009). The impact of volcanic forcing on tropical temperatures during the past four centuries. *Nature Geoscience*, 2(1), 51–56. <https://doi.org/10.1038/ngeo393>
- Devine, J. D., Gardner, J. E., Brack, H. P., Layne, G. D., & Rutherford, M. J. (1995a). Comparison of microanalytical methods for estimating H₂O contents of silicic volcanic glasses. *American Mineralogist*, 80(3–4), 319–328. <https://doi.org/10.2138/am-1995-3-413>
- Devine, J. D., Gardner, J. E., Brack, H. P., Layne, G. D., & Rutherford, M. J. (1995b). Comparison of microanalytical methods for estimating H₂O contents of silicic volcanic glasses. *American Mineralogist*, 80(3), 319–328.
- Di Roberto, A., Bertagnini, A., Del Carlo, P., Meletlidis, S., & Pompilio, M. (2016). The 1909 Chinyero eruption on Tenerife (Canary Islands): Insights from historical accounts, and tephrostratigraphic and geochemical data. *Bulletin of Volcanology*, 78(12), 88. <https://doi.org/10.1007/s00445-016-1083-7>
- Engwell, S. L., Aspinall, W. P., & Sparks, R. S. J. (2015). An objective method for the production of isopach maps and implications for the estimation of tephra deposit volumes and their uncertainties. *Bulletin of Volcanology*, 77(61), 1–18. <https://doi.org/10.1007/s00445-015-0942-y>
- Forbes, A. E., Blake, S., Tuffen, H., & Wilson, A. (2014). Fractures in a trachyandesitic lava at Öræfajökull, Iceland, used to infer subglacial emplacement in 1727–8 eruption. *Journal of Volcanology and Geothermal Research*, 288, 8–18. <https://doi.org/10.1016/j.jvolgeores.2014.10.004>

- Gao, C., Robock, A., & Ammann, C. (2008). Volcanic forcing of climate over the past 1500 years: An improved ice core-based index for climate models. *Journal of Geophysical Research*, 113(D23), D23111. <https://doi.org/10.1029/2008jd010239>
- Glaze, L. S., Self, S., Schmidt, A., & Hunter, S. J. (2017). Assessing eruption column height in ancient flood basalt eruptions. *Earth and Planetary Science Letters*, 457, 263–270. <https://doi.org/10.1016/j.epsl.2014.07.043>
- Gómez-Ortiz, D., Montesinos, F. G., Martín-Crespo, T., Solla, M., Arnosó, J., & Vélez, E. (2014). Combination of geophysical prospecting techniques into areas of high protection value: Identification of shallow volcanic structures. *Journal of Applied Geophysics*, 109, 15–26. <https://doi.org/10.1016/j.jappgeo.2014.07.009>
- Gómez-Ulla, A., Edmonds, M., & Sigmarsson, O. (2019). Elevated CO₂ concentrations and volatile-trace element ratios suggest carbon-rich fluid flux melting under Lanzarote, Canary Islands. *Geophysical Research Abstracts*, 21.
- Gómez-Ulla, A., Sigmarsson, O., & Gudfinnsson, G. H. (2017). Trace element systematics of olivine from historical eruptions of Lanzarote, Canary Islands: Constraints on mantle source and melting mode. *Chemical Geology*, 449, 99–111. <https://doi.org/10.1016/j.chemgeo.2016.11.021>
- Gómez-Ulla, A., Sigmarsson, O., Huertas, M. J., Devidal, J.-L., & Ancochea, E. (2018). The historical basanite-alkali basalt-tholeiite suite at Lanzarote, Canary Islands: Carbonated melts of heterogeneous mantle source? *Chemical Geology*, 494, 56–68. <https://doi.org/10.1016/j.chemgeo.2018.07.015>
- Gudmundsson, M. T., Jónsdóttir, K., Hooper, A., Holohan, E. P., Halldórsson, S. A., Ófeigsson, B. G., Cesca, S., Vogfjörð, K. S., Sigmundsson, F., Högnadóttir, T., Einarsson, P., Sigmarsson, O., Jarosch, A. H., Jónasson, K., Magnússon, E., Hreinsdóttir, S., Bagnardi, M., Parks, M. M., Hjörleifsdóttir, V., ... Aiuppa, A. (2016). Gradual caldera collapse at Bárðarbunga volcano, Iceland, regulated by lateral magma outflow. *Science*, 353(6296), 262. <https://doi.org/10.1126/science.aaf8988>
- Guo, S., Bluth, G. J. S., Rose, W. I., Watson, I. M., & Prata, A. J. (2004). Re-evaluation of SO₂ release of the 15 June 1991 Pinatubo eruption using ultraviolet and infrared satellite sensors. *Geochemistry, Geophysics, Geosystems*, 5(4), Q04001. <https://doi.org/10.1029/2003GC000654>
- Hammer, C. U., Clausen, H. B., & Dansgaard, W. (1980). Greenland ice sheet evidence of post-glacial volcanism and its climatic impact. *Nature*, 288(5788), 230–235. <https://doi.org/10.1038/288230a0>
- Hartley, M. E., Maclennan, J., Edmonds, M., & Thordarson, T. (2014). Reconstructing the deep CO₂ degassing behaviour of large basaltic fissure eruptions. *Earth and Planetary Science Letters*, 393, 120–131. <https://doi.org/10.1016/j.epsl.2014.02.031>
- Hayer, C., Barrancos, J., Burton, M., Rodríguez, F., Esse, B., Hernández, P., Melián, G., Padrón, E., Asensio-Ramos, M., & Pérez, N. (2022). *From up above to down below: Comparison of satellite- and ground-based observations of SO₂ emissions from the 2021 eruption of Cumbre Vieja, La Palma*. EGU22-12201. <https://doi.org/10.5194/egusphere-egu22-12201>
- Hevia, A., Sánchez-Salguero, R., Camarero, J. J., Buras, A., Sangüesa-Barreda, G., Galván, J. D., & Gutiérrez, E. (2018). Towards a better understanding of long-term wood-chemistry variations in old-growth forests: A case study on ancient *Pinus uncinata* trees from the Pyrenees. *Science of the Total Environment*, 625, 220–232. <https://doi.org/10.1016/j.scitotenv.2017.12.229>
- Hill, B. E., Connor, C. B., Jarzempa, M. S., La Femina, P. C., Navarro, M., & Strauch, W. (1998). 1995 eruptions of Cerro Negro Volcano, Nicaragua, and risk assessment for future eruptions. *GSA Bulletin*, 110(10), 1231–1241. [https://doi.org/10.1130/0016-7606\(1998\)110<1231:EOCNVN>2.3.CO;2](https://doi.org/10.1130/0016-7606(1998)110<1231:EOCNVN>2.3.CO;2)
- Houghton, B. F., & Wilson, C. J. N. (1989). A vesicularity index for pyroclastic deposits. *Bulletin of Volcanology*, 51, 451–462. <https://doi.org/10.1007/BF01078811>

- Jahn, R., & Stahr, K. (1996). Development of soils and site qualities on basic volcanoclastics with special reference to the semiarid environment of Lanzarote, Canary Islands, Spain. *Revista Mexicana de Ciencias Geológicas*, 13(1), 104–112.
- Jarosewich, E. (2002). Smithsonian microbeam standards. *Journal of Research of the National Institute of Standards and Technology*, 107(6), 681–685. <https://doi.org/10.6028/jres.107.054>
- Jochum, K. P., & Nohl, U. (2008). Reference materials in geochemistry and environmental research and the GeoReM database. *Chemical Geology*, 253(1), 50–53. <https://doi.org/10.1016/j.chemgeo.2008.04.002>
- Johnson, D., Hooper, P., & Conrey, R. (1999). XRF analysis of rocks and minerals for major and trace elements on a single low dilution Li-tetraborate fused bead. *Advances in X-Ray Analysis*, 41, 843–867.
- Kervyn, M., Ernst, G. G. J., Carracedo, J. C., & Jacobs, P. (2012). Geomorphometric variability of “monogenetic” volcanic cones: Evidence from Mauna Kea, Lanzarote and experimental cones. *Geomorphology*, 136(1), 59–75. <https://doi.org/10.1016/j.geomorph.2011.04.009>
- Knaack, C., Cornelius, S., & Hooper, P. R. (1994). Trace element analyses of rocks and minerals by ICP-MS. *Open File Report, Department of Geology, Washington State University*.
- Kueppers, U., Scheu, B., Spieler, O., & Dingwell, D. B. (2005). Field-based density measurements as tool to identify preeruption dome structure: Set-up and first results from Unzen volcano, Japan. *Journal of Volcanology and Geothermal Research*, 141(1–2), 65–75. <https://doi.org/10.1016/j.jvolgeores.2004.09.005>
- Le Bas, M. J., Le Maitre, R. W., Streckeisen, A., & Zanettin, B. (1986). A chemical classification of volcanic rocks based on the total alkali-silica diagram. *Journal of Petrology*, 27(3), 745–750. <https://doi.org/10.1093/petrology/27.3.745>
- Longpré, M.-A., & Felpeto, A. (2021). Historical volcanism in the Canary Islands; part 1: A review of precursory and eruptive activity, eruption parameter estimates, and implications for hazard assessment. *Journal of Volcanology and Geothermal Research*, 419, 107363. <https://doi.org/10.1016/j.jvolgeores.2021.107363>
- Longpré, M.-A., Stix, J., Costa, F., Espinoza, E., & Muñoz, A. (2014). Magmatic processes and associated timescales leading to the January 1835 eruption of Cosigüina volcano, Nicaragua. *Journal of Petrology*, 55(6), 1173–1201. <https://doi.org/10.1093/petrology/egu022>
- Longpré, M.-A., Stix, J., Klügel, A., & Shimizu, N. (2017). Mantle to surface degassing of carbon- and sulphur-rich alkaline magma at El Hierro, Canary Islands. *Earth and Planetary Science Letters*, 460, 268–280. <https://doi.org/10.1016/j.epsl.2016.11.043>
- Lundstrom, C. C., Hoernle, K., & Gill, J. (2003). U-series disequilibria in volcanic rocks from the Canary Islands: Plume versus lithospheric melting. *Geochimica et Cosmochimica Acta*, 67(21), 4153–4177. [https://doi.org/10.1016/s0016-7037\(03\)00308-9](https://doi.org/10.1016/s0016-7037(03)00308-9)
- Mani, L., Tzachor, A., & Cole, P. (2021). Global catastrophic risk from lower magnitude volcanic eruptions. *Nature Communications*, 12(1), 4756. <https://doi.org/10.1038/s41467-021-25021-8>
- Martí, J., Planagumà, L. I., Geyer, A., Aguirre-Díaz, G., Pedrazzi, D., & Bolós, X. (2017). Basaltic ignimbrites in monogenetic volcanism: The example of La Garrotxa volcanic field. *Bulletin of Volcanology*, 79, 1–12. <https://doi.org/10.1007/s00445-017-1113-0>
- McDonough, W. F., & Sun, S. -s. (1995). The composition of the Earth. *Chemical Geology*, 120(3–4), 223–253. [https://doi.org/10.1016/0009-2541\(94\)00140-4](https://doi.org/10.1016/0009-2541(94)00140-4)
- Menand, T., & Tait, S. R. (2001). A phenomenological model for precursor volcanic eruptions. *Nature*, 411(6838), 678–680. <https://doi.org/10.1038/35079552>

- Michael, P. (1995). Regionally distinctive sources of depleted MORB: evidence from trace elements and H₂O. *Earth and Planetary Science Letters*, 131(3), 301–320. [https://doi.org/10.1016/0012-821X\(95\)00023-6](https://doi.org/10.1016/0012-821X(95)00023-6)
- Michael, P. J., & Graham, D. W. (2015). The behavior and concentration of CO₂ in the suboceanic mantle: Inferences from undegassed ocean ridge and ocean island basalts. *Lithos*, 236–237, 338–351. <https://doi.org/10.1016/j.lithos.2015.08.020>
- Neal, C. A., Brantley, S. R., Antolik, L., Babb, J. L., Burgess, M., Calles, K., Cappos, M., Chang, J. C., Conway, S., Desmither, L., Dotray, P., Elias, T., Fukunaga, P., Fuke, S., Johanson, I. A., Kamibayashi, K., Kauahikaua, J., Lee, R. L., Pekalib, S., ... Damby, D. (2019). The 2018 rift eruption and summit collapse of Kīlauea Volcano. *Science*, 363(6425), 367–374. <https://doi.org/10.1126/science.aav7046>
- Newhall, C. G., & Self, S. (1982). The Volcanic Explosivity Index (VEI): An estimate of explosive magnitude for historical volcanism. *Journal of Geophysical Research*, 87(C2), 1231–1238. <https://doi.org/10.1029/JC087iC02p01231>
- PAGES 2k Consortium. (2013). Continental-scale temperature variability during the past two millennia. *Nature Geoscience*, 6(5), 339–346. <https://doi.org/10.1038/ngeo1797>
- Pallarés Padilla, A. (2007). Nuevas aportaciones al conocimiento de la erupción de Timanfaya (Lanzarote). *Académico de Número, Academia de Ciencias e Ingenierías de Lanzarote*, 45.
- Palme, H., & O'Neill, H. S. C. (2003). Cosmochemical estimates of mantle composition. *Treatise on Geochemistry*, 2, 1–38. <https://doi.org/10.1016/B0-08-043751-6/02177-0>
- Pedersen, G. B. M., Höskuldsson, A., Dürig, T., Thordarson, T., Jonsdottir, I., Riishuus, M. S., Óskarsson, B. V., Dumont, S., Magnússon, E., & Gudmundsson, M. T. (2017). Lava field evolution and emplacement dynamics of the 2014–2015 basaltic fissure eruption at Holuhraun, Iceland. *Journal of Volcanology and Geothermal Research*, 340, 155–169. <https://doi.org/10.1016/j.jvolgeores.2017.02.027>
- Perez-Torrado, F. J., Carracedo, J. C., Guillou, H., Rodriguez-Gonzalez, A., & Fernandez-Turiel, J. L. (2023). Age, duration and spatial distribution of ocean shields and rejuvenated volcanism: Fuerteventura and Lanzarote, Eastern Canaries. *Journal of the Geological Society*, 180(4), jgs2022-112. <https://doi.org/10.1144/jgs2022-112>
- Pioli, L., Erlund, E., Johnson, E., Cashman, K., Wallace, P., Rosi, M., & Delgado Granados, H. (2008). Explosive dynamics of violent Strombolian eruptions: The eruption of Parícutin Volcano 1943–1952 (Mexico). *Earth and Planetary Science Letters*, 271(1–4), 359–368. <https://doi.org/10.1016/j.epsl.2008.04.026>
- Pyle, D. M. (1989). The thickness, volume and grain size of tephra fall deposits. *Bulletin of Volcanology*, 51(1), 1–15. <https://doi.org/10.1007/BF01086757>
- Pyle, D. M. (2015). Sizes of volcanic eruptions. In H. Sigurdsson (Ed.), *The Encyclopedia of Volcanoes (Second Edition)* (pp. 257–264). Academic Press. <https://www.sciencedirect.com/science/article/pii/B9780123859389000134>
- Reiners, P. W. (2002). Temporal-compositional trends in intraplate basalt eruptions: Implications for mantle heterogeneity and melting processes. *Geochemistry, Geophysics, Geosystems*, 3(2), 1–30. <https://doi.org/10.1029/2001GC000250>
- Robock, A. (2000). Volcanic eruptions and climate. *Reviews of Geophysics*, 38(2), 191–219. <https://doi.org/10.1029/1998rg000054>
- Rodríguez, F., Martín-Lorenzo, Alba, Coldwell, Beverley, Andronico, Daniele, Bonadonna, Costanza, Del Bello, Elisabetta, Pistolesi, Marco, Taddeucci, Jacopo, Biass, Sebastien, E. Romero, Jorge, Voloschina, Marija, Scarlato, Piergiorgio, Hernandez, William, Longpré, Marc-Antoine, Cohen,

Maia, D'Auria, Luca, M. Pérez, Nemesio, & Pankhurst, Matthew J. (submitted). *Tephra stratigraphy of the 2021 Tajogaite eruption of Cumbre Vieja, La Palma, Canary Islands*.

- Romero, C. (2003). *El relieve de Lanzarote*. Servicio de Publicaciones, Cabildo de Lanzarote.
- Rosenthal, A., Hauri, E. H., & Hirschmann, M. M. (2015). Experimental determination of C, F, and H partitioning between mantle minerals and carbonated basalt, CO₂/Ba and CO₂/Nb systematics of partial melting, and the CO₂ contents of basaltic source regions. *Earth and Planetary Science Letters*, 412(0), 77–87. <https://doi.org/10.1016/j.epsl.2014.11.044>
- Rowland, S. K., Jurado-Chichay, Z., Ernst, G., & Walker, G. P. L. (2009). Pyroclastic deposits and lava flows from the 1759–1774 eruption of El Jorullo, México: Aspects of 'violent Strombolian' activity and comparison with Parícutin. In T. Thordarson, S. Self, G. Larsen, S. K. Rowland, & Á. Höskuldsson (Eds.), *Studies in Volcanology: The Legacy of George Walker* (Vol. 2, p. 0). Geological Society of London. <https://doi.org/10.1144/IAVCEI002.6>
- Rubin, A. M. (1995). Propagation of magma-filled cracks. *Annual Review of Earth and Planetary Sciences*, 23, 287–336. <https://doi.org/10.1146/annurev.ea.23.050195.001443>
- Saal, A. E., Hauri, E. H., Langmuir, C. H., & Perfit, M. R. (2002). Vapour undersaturation in primitive mid-ocean-ridge basalt and the volatile content of Earth's upper mantle. *Nature*, 419(6906), 451–455. <https://doi.org/10.1038/nature01073>
- Salzer, M. W., & Hughes, M. K. (2007). Bristlecone pine tree rings and volcanic eruptions over the last 5000 yr. *Quaternary Research*, 67(1), 57–68. <https://doi.org/10.1016/j.yqres.2006.07.004>
- Scandone, R., Bartolini, S., & Martí, J. (2016). A scale for ranking volcanoes by risk. *Bulletin of Volcanology*, 78, 2. <https://doi.org/10.1007/s00445-015-0995-y>
- Schmincke, H.-U., Klügel, A., Hansteen, T. H., Hoernle, K., & van den Bogaard, P. (1998). Samples from the Jurassic ocean crust beneath Gran Canaria, La Palma and Lanzarote (Canary Islands). *Earth and Planetary Science Letters*, 163(1–4), 343–360. [https://doi.org/10.1016/S0012-821X\(98\)00168-X](https://doi.org/10.1016/S0012-821X(98)00168-X)
- Self, S., Widdowson, M., Thordarson, T., & Jay, A. E. (2006). Volatile fluxes during flood basalt eruptions and potential effects on the global environment: A Deccan perspective. *Earth and Planetary Science Letters*, 248(1–2), 518–532. <https://doi.org/10.1016/j.epsl.2006.05.041>
- Sharma, K., Blake, S., & Self, S. (2005). Quantifying sulphur emissions and atmospheric aerosol loading from the 1730–36 Lanzarote eruption. *Eos Trans. AGU*, 86(52), Fall Meet. Suppl., Abstract V21E-0672.
- Sides, I. R., Edmonds, M., Maclennan, J., Swanson, D. A., & Houghton, B. F. (2014). Eruption style at Kilauea Volcano in Hawai'i linked to primary melt composition. *Nature Geoscience*, 7(6), 464–469. <https://doi.org/10.1038/ngeo2140>
- Sigl, M., Winstrup, M., McConnell, J. R., Welten, K. C., Plunkett, G., Ludlow, F., Buntgen, U., Caffee, M., Chellman, N., Dahl-Jensen, D., Fischer, H., Kipfstuhl, S., Kostick, C., Maselli, O. J., Mekhaldi, F., Mulvaney, R., Muscheler, R., Pasteris, D. R., Pilcher, J. R., ... Woodruff, T. E. (2015). Timing and climate forcing of volcanic eruptions for the past 2,500 years. *Nature*, 523(7562), 543–549. <https://doi.org/10.1038/nature14565>
- Sigmarsson, O., Carn, S., & Carracedo, J. C. (1998). Systematics of U-series nuclides in primitive lavas from the 1730–36 eruption on Lanzarote, Canary Islands, and implications for the role of garnet pyroxenites during oceanic basalt formations. *Earth and Planetary Science Letters*, 162(1), 137–151. [https://doi.org/10.1016/S0012-821X\(98\)00162-9](https://doi.org/10.1016/S0012-821X(98)00162-9)
- Solana, M. C., Kilburn, C. R. J., Rodríguez Badiola, E., & Aparicio, A. (2004). Fast emplacement of extensive pahoehoe flow-fields: The case of the 1736 flows from Montaña de las Nueces, Lanzarote. *Journal of Volcanology and Geothermal Research*, 132(2–3), 189–207. [https://doi.org/10.1016/S0377-0273\(03\)00345-7](https://doi.org/10.1016/S0377-0273(03)00345-7)

- Soule, A., Heffron, E., Gee, L., Mayer, L., Raineault, N. A., German, C. R., Lim, D., Zoeller, M. H., & Parcheta, C. (2019). Mapping the lava deltas of the 2018 eruption of Kīlauea Volcano. *Oceanography*, 32(1), 46–47. USGS Publications Warehouse. <https://doi.org/10.5670/oceanog.2019.supplement.01>
- Stix, J., Gauthier, G., & Ludden, J. N. (1995). A critical look at quantitative laser-ablation ICP-MS analysis of natural and synthetic glasses. *The Canadian Mineralogist*, 33(2), 435–444.
- Taracsák, Z., Hartley, M. E., Burgess, R., Edmonds, M., Iddon, F., & Longpré, M.-A. (2019). High fluxes of deep volatiles from ocean island volcanoes: Insights from El Hierro, Canary Islands. *Geochimica et Cosmochimica Acta*, 258, 19–36. <https://doi.org/10.1016/j.gca.2019.05.020>
- Thomas, L. E., Hawkesworth, C. J., Van Calsteren, P., Turner, S. P., & Rogers, N. W. (1999). Melt generation beneath ocean islands: A U-Th-Ra isotope study from Lanzarote in the Canary Islands. *Geochimica et Cosmochimica Acta*, 63(23–24), 4081–4099. [https://doi.org/10.1016/s0016-7037\(99\)00310-5](https://doi.org/10.1016/s0016-7037(99)00310-5)
- Thordarson, T., & Larsen, G. (2007). Volcanism in Iceland in historical time: Volcano types, eruption styles and eruptive history. *Journal of Geodynamics*, 43(1), 118–152. <https://doi.org/10.1016/j.jog.2006.09.005>
- Thordarson, T., & Self, S. (1993). The Laki (Skaftár Fires) and Grímsvötn eruptions in 1783–1785. *Bulletin of Volcanology*, 55(4), 233–263. <https://doi.org/10.1007/BF00624353>
- Thordarson, T., & Self, S. (2003). Atmospheric and environmental effects of the 1783–1784 Laki eruption: A review and reassessment. *Journal of Geophysical Research: Atmospheres*, 108(D1), 4011. <https://doi.org/10.1029/2001JD002042>
- Thordarson, T., Self, S., Oskarsson, N., & Hulsebosch, T. (1996). Sulfur, chlorine, and fluorine degassing and atmospheric loading by the 1783–1784 AD Laki (Skaftár Fires) eruption in Iceland. *Bulletin of Volcanology*, 58(2), 205–225.
- Thordarson, T., Self, S., Óskarsson, N., & Hulsebosch, T. (1996). Sulfur, chlorine, and fluorine degassing and atmospheric loading by the 1783–1784 AD Laki (Skaftár Fires) eruption in Iceland. *Bulletin of Volcanology*, 58(2), 205–225. <https://doi.org/10.1007/s004450050136>
- Toohey, M., & Sigl, M. (2017). Volcanic stratospheric sulfur injections and aerosol optical depth from 500 BCE to 1900 CE. *Earth System Science Data*, 9(2), 809–831. <https://doi.org/10.5194/essd-9-809-2017>
- Troll, V. R., Carracedo, J. C., Jägerup, B., Streng, M., Barker, A. K., Deegan, F. M., Perez-Torrado, F., Rodriguez-Gonzalez, A., & Geiger, H. (2017). Volcanic particles in agriculture and gardening. *Geology Today*, 33(4), 148–154. <https://doi.org/10.1111/gto.12193>
- Troll, V. R., Klügel, A., Longpré, M.-A., Burchardt, S., Deegan, F. M., Carracedo, J. C., Wiesmaier, S., Kueppers, U., Dahren, B., Blythe, L. S., Hansteen, T. H., Freda, C., Budd, D. A., Jolis, E. M., Jonsson, E., Meade, F. C., Harris, C., Berg, S. E., Mancini, L., ... Pedroza, K. (2012). Floating stones off El Hierro, Canary Islands: Xenoliths of pre-island sedimentary origin in the early products of the October 2011 eruption. *Solid Earth*, 3(1), 97–110. <https://doi.org/10.5194/se-3-97-2012>
- Valentine, G. A., & Gregg, T. K. P. (2008). Continental basaltic volcanoes—Processes and problems. *Journal of Volcanology and Geothermal Research*, 177(4), 857–873. <https://doi.org/10.1016/j.jvolgeores.2008.01.050>
- van den Bogaard, P. (2013). The origin of the Canary Island Seamount Province—New ages of old seamounts. *Scientific Reports*, 3, 2107. <https://doi.org/10.1038/srep02107>
- von Suchodoletz, H., Fuchs, M., & Zöller, L. (2008). Dating Saharan dust deposits on Lanzarote (Canary Islands) by luminescence dating techniques and their implication for palaeoclimate reconstruction

of NW Africa. *Geochemistry, Geophysics, Geosystems*, 9(2), Q02Q07.
<https://doi.org/10.1029/2007GC001658>

Walker, G. P. L., Self, S., & Wilson, L. (1984). Tarawera 1886, New Zealand—A basaltic plinian fissure eruption. *Journal of Volcanology and Geothermal Research*, 21(1–2), 61–78.
[https://doi.org/10.1016/0377-0273\(84\)90016-7](https://doi.org/10.1016/0377-0273(84)90016-7)

White, J. D. L., & Houghton, B. F. (2006). Primary volcanoclastic rocks. *Geology*, 34(8), 677–680.
<https://doi.org/10.1130/g22346.1>

Zaczek, K., Troll, V. R., Cachao, M., Ferreira, J., Deegan, F. M., Carracedo, J. C., Soler, V., Meade, F. C., & Burchardt, S. (2015). Nanofossils in 2011 El Hierro eruptive products reinstate plume model for Canary Islands. *Scientific Reports*, 5, 7945. <https://doi.org/10.1038/srep07945>

Zielinski, G. A. (1995). Stratospheric loading and optical depth estimates of explosive volcanism over the last 2100 years derived from the Greenland Ice Sheet Project 2 ice core. *Journal of Geophysical Research*, 100(D10), 20937–20955. <https://doi.org/10.1029/95jd01751>

FIGURES

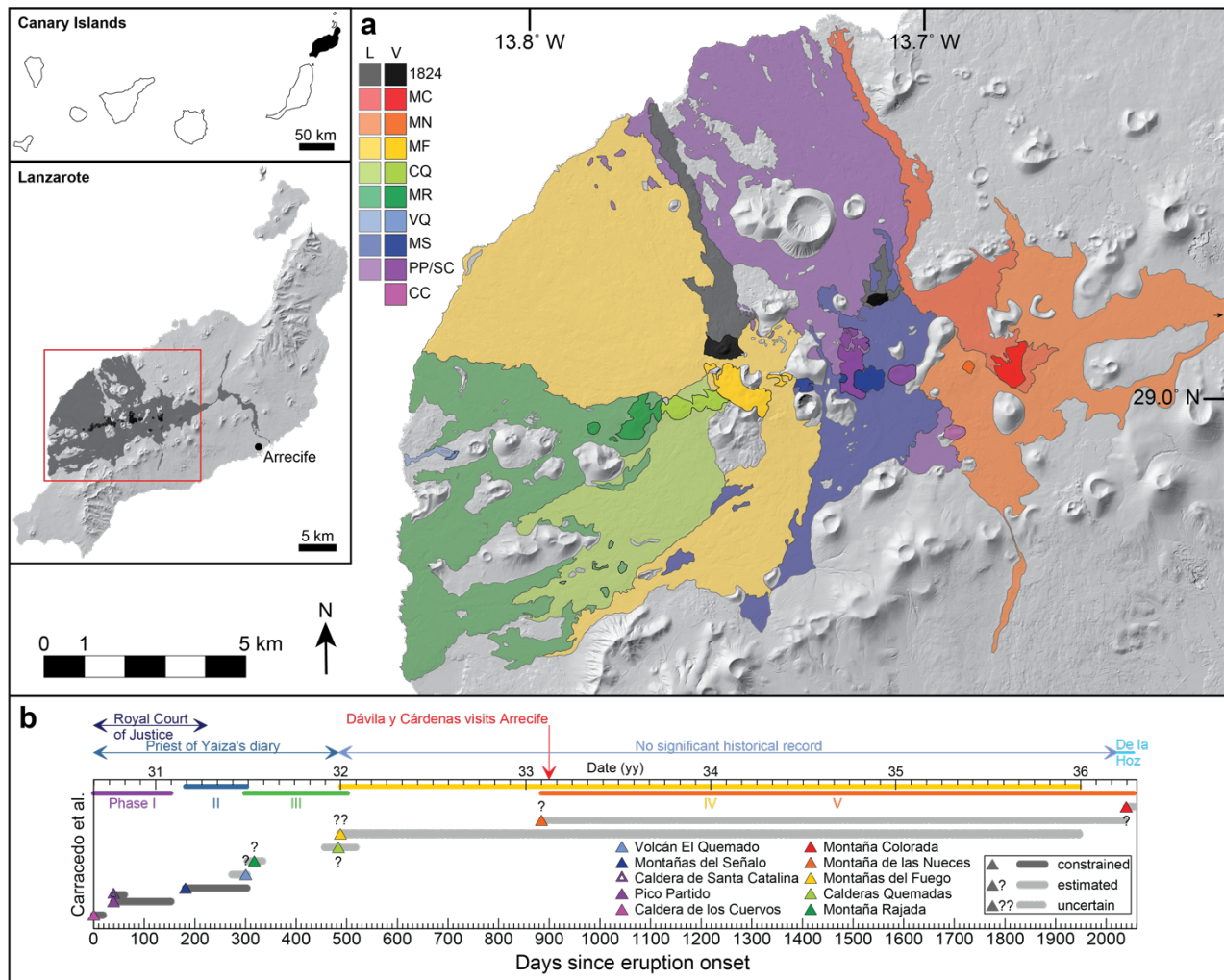


Figure 1. Map of Timanfaya lava flows and eruption timeline. (a) Digital elevation model of Lanzarote showing the 1730–1736 lava flows (L) and the location of associated source vents (V), after Carracedo and Rodríguez Badiola (1991). The color code refers to the eruption timeline in (b): CC: Caldera de los Cuervos; PP/SC: Pico Partido and Caldera de Santa Catalina; MS: Montañas del Señalo; VQ: Volcán El Quemado; MR: Montaña Rajada; CQ: Calderas Quemadas; MF: Montañas del Fuego; MN: Montaña de las Nueces; MC: Montaña Colorada. First inset: Map of the Canary Islands with Lanzarote shown in black. Second inset: Map of Lanzarote showing the full extent of the 1730–1736 flow field in gray and the area expanded in (a) (red rectangle). (b) Eruption timeline modified after Longpré and Felpeto (2021), based on historical records and geologic mapping (Carracedo et al., 1990, 1992; Carracedo & Rodríguez Badiola, 1991).

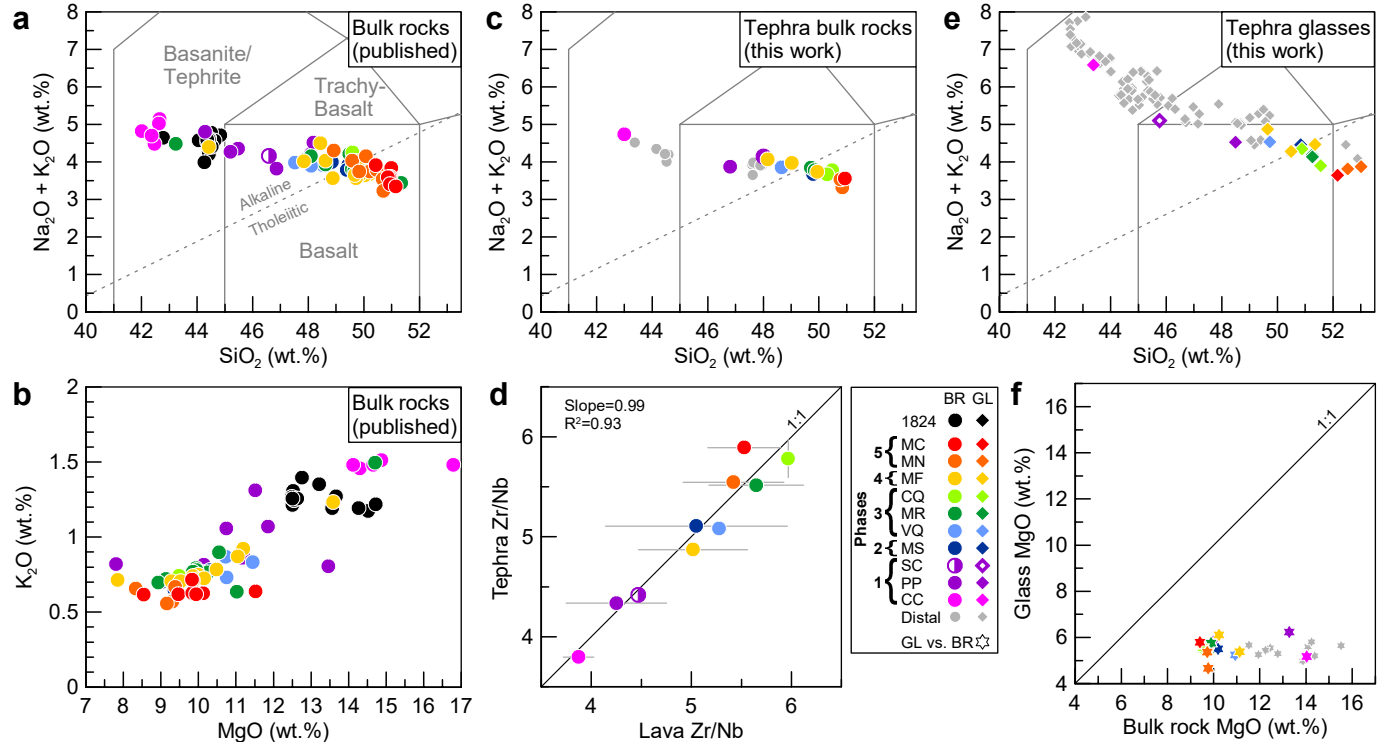


Figure 2. The temporal-compositional trend of Timanfaya lavas and tephtras. (a) Total alkalis vs. silica diagram (TAS) (Le Bas et al., 1986) and (b) K₂O vs. MgO contents for published bulk rock data (Carracedo et al., 1990; Gómez-Ulla et al., 2017; Thomas et al., 1999), defining the early, high-MgO basanite to late tholeiite trend. (c) TAS diagram for bulk rocks of vent tephtras and representative distal tephtras presented in this work. (d) Comparison of the Zr/Nb ratios of vent tephtras (this work) with that of lavas reported by Carracedo et al. (1990), showing excellent correspondence. Error bars are one standard deviation of the mean of multiple analyses. (e) TAS diagram for matrix glasses of vent and distal tephtras (this work), revealing the alkaline character of the majority of distal tephtras. Each data point represents 1–7 EPMA analyses. (f) Comparison of the MgO content of matrix glasses with that of corresponding bulk rocks for our tephtra samples, showing a large discrepancy due to the olivine-rich crystal cargo of Timanfaya tephtras. Sample type: BR: bulk rock; GL: matrix glass. Sample identification: CC: Caldera de los Cuervos; PP: Pico Partido; SC: Caldera de Santa Catalina; MS: Montañas del Señalo; VQ: Volcán El Quemado; MR: Montaña Rajada; CQ: Calderas Quemadas; MF: Montañas del Fuego; MN: Montaña de las Nueces; MC: Montaña Colorada (see Figure 1); distal: distal tephtras from stratigraphic sections.

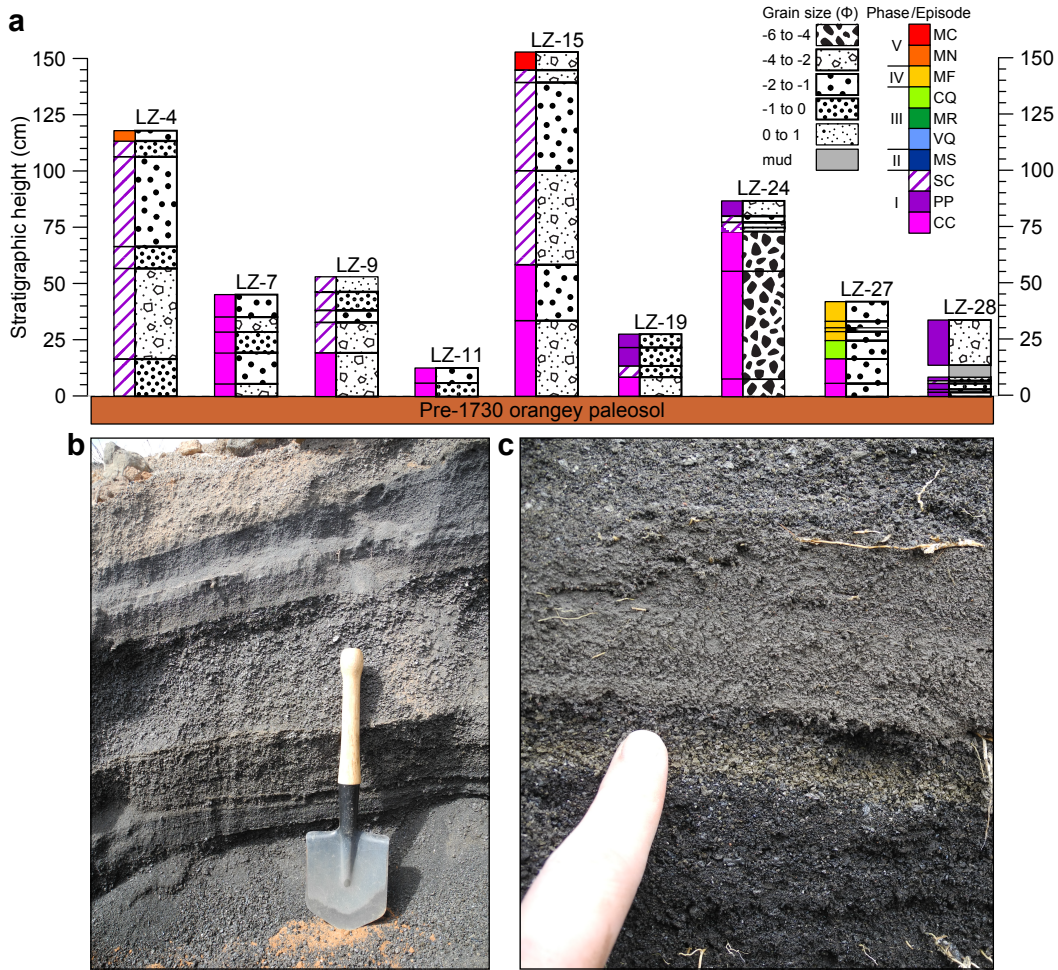


Figure 3. Stratigraphy of Timanfaya tephras. (a) Stratigraphic columns of selected trench localities show grain size, as average clast diameter from each bed. Colored bars on the left-hand side indicate corresponding source vent, as determined by geochemical correlation. (b) Picture of representative section (near site LZ-4), with an orangey paleosol at its base, interbedded lapilli and ash in the middle, and an upper brownish layer interpreted to be reworked. Shovel is 50-cm-long for scale. (c) Close-up on the upper part of the same section showing a thin layer of distinctive golden frothy lapilli resembling those found on the flanks Montaña Colorada.

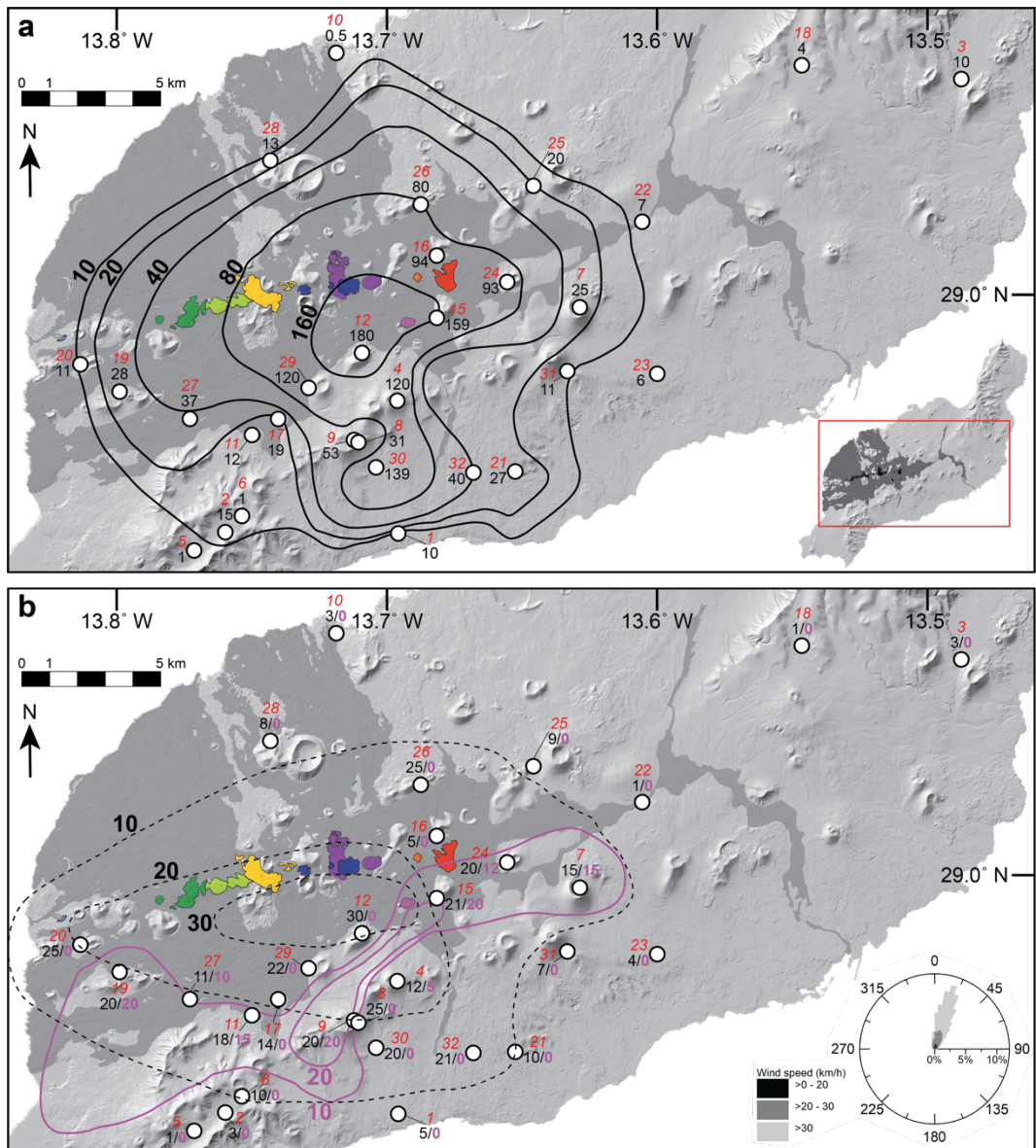


Figure 4. Isopach and isopleth maps. (a) Isopach map showing total tephra deposit thickness, with 10, 20, 40, 80, and 160 cm contours (bold type). Individual field sites are indicated by a white circle, with a two-digit label. The digit in red italic type is the site number, and the digit in black type is the total tephra thickness in cm. Inset: Map of Lanzarote showing the area expanded in this figure (red rectangle). (b) Map showing two sets of isopleths for maximum clast size (in mm), one for the total deposit (black dashed lines and bold type) and the other focusing on a particularly coarse and thick basal bed tied to Caldera de los Cuervos based on stratigraphic position and geochemical composition (magenta solid lines and bold type). Site labels record site number (red italic) and maximum clast size (total deposit: black type; basal bed only: magenta bold type). Inset: Rose diagram showing wind directions and speed at 100 m altitude near Arrecife, from 2000 to 2020. Data from open-meteo.com. In both (a) and (b), the location of the 1730–1736 lava flow (gray) and main vents are shown for reference (see Fig. 1).

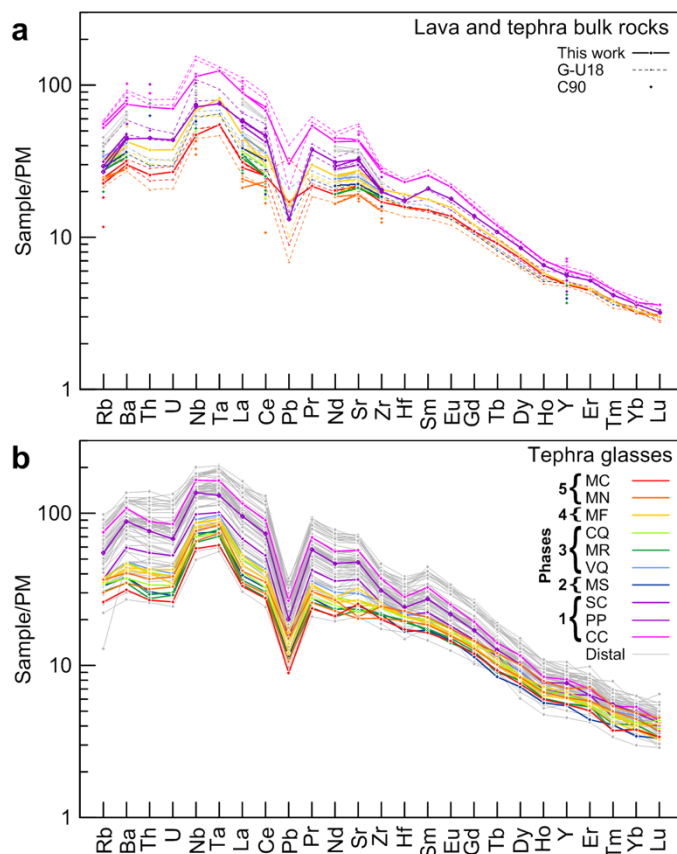


Figure 5. Primitive mantle-normalized multi-element diagrams. (a) Comparison of bulk rock samples from Gómez-Ulla et al. (2018) (G-U18) and Carracedo et al. (1990) (C90) and this work. Th and U values obtained by XRF were omitted due to low precision. (b) Matrix glass data for both vent (colored lines) and distal (gray lines) tephtras, showing the enriched nature of distal tephtras resembling the compositions of Caldera de los Cuervos, Pico Partido and Caldera de Santa Catalina tephtras. Most distal tephtras also show strong positive Nb anomalies and negative Pb, Zr and Hf anomalies. Primitive mantle (PM) values are those of McDonough and Sun (1995).

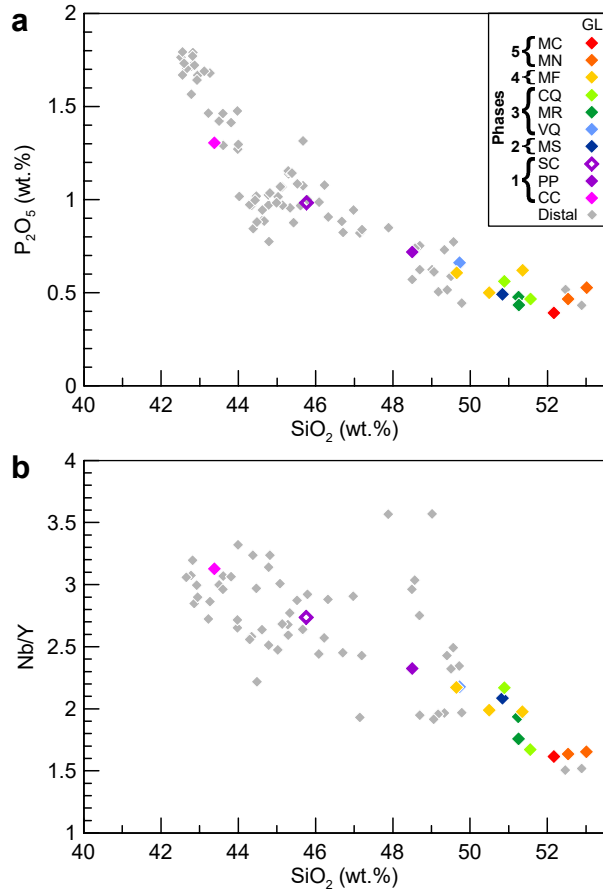


Figure 6. Distal tephra–source vent correlation plots. (a) P₂O₅ and (b) Nb/Y against SiO₂ content for distal and vent tephra glasses. Distal tephra are matched to their corresponding source vent based on Euclidean distance minima.

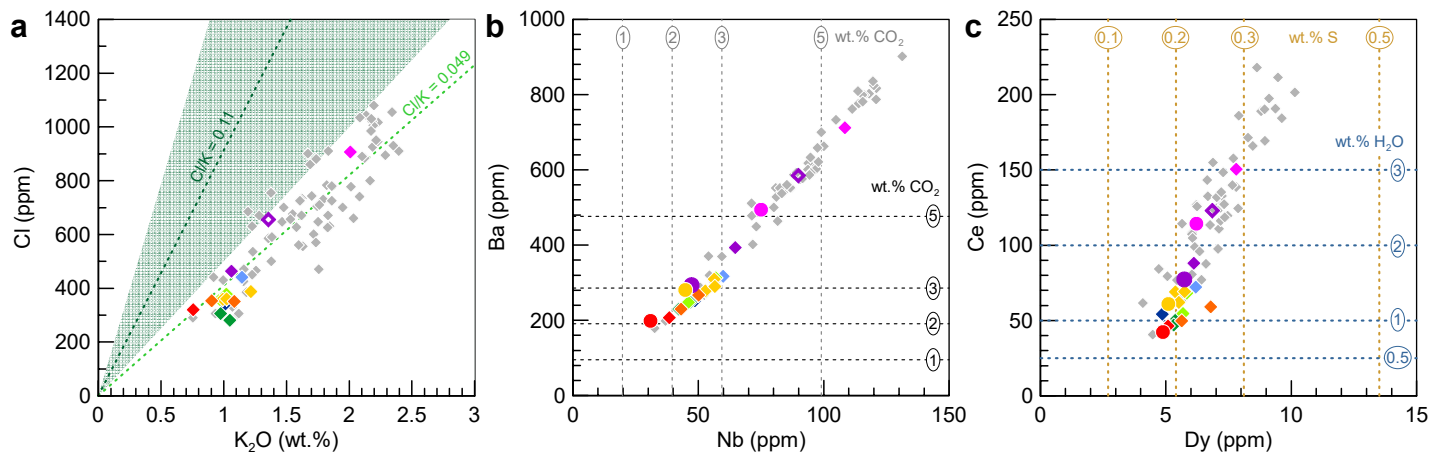


Figure 7. Volatiles and trace element proxies. (a) Cl and K_2O contents in Timanfaya matrix glasses, defining a Cl/K ratio of 0.049, which is lower than the Primitive Mantle value of 0.11 (with a one standard deviation range of 0.06–0.19 shown by the shaded green envelope) proposed by Palme and O'Neill (2003). (b) Ba and Nb concentrations as proxies for undegassed CO_2 content. Horizontal and vertical dashed lines denote predicted CO_2 contents (circled numbers, in wt.%) assuming mantle CO_2/Ba and CO_2/Nb ratios of 105 (Michael & Graham, 2015) and 505 (Rosenthal et al., 2015), respectively. (c) Ce and Dy concentrations as proxies for undegassed H_2O and S contents, respectively. Predicted H_2O contents based on a H_2O/Ce ratio of 200 (Michael, 1995; Saal et al., 2002) are shown by horizontal dashed lines, whereas vertical dashed lines mark predicted S concentrations using a S/Dy ratio of 370 (McDonough & Sun, 1995).

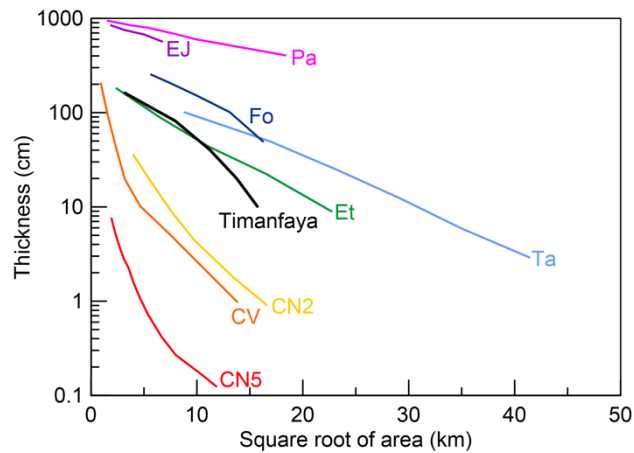


Figure 8. Tephra deposit thickness versus square root of isopach area. The Timanfaya tephra blanket is compared with other basaltic eruptions, including long-lasting cone-forming eruptions [Pa: 1943–1952 Paricutin, (Pioli et al., 2008); EJ: 1759–1774 El Jorullo (Rowland et al., 2009); CV: 2021 Cumbre Vieja (Bonadonna et al., 2022)], Plinian eruptions [Fo: 60 ka Fontana Lapilli (Costantini et al., 2009); Ta: 1886 Tarawera (Walker et al., 1984); Et: 122 BC Etna (Coltelli et al., 1998)] and two contrasting eruptions of Cerro Negro, Nicaragua [CN2: 1992 VEI 3 (Connor & Connor, 2006); CN5: 1995 VEI 2 (Hill et al., 1998)].

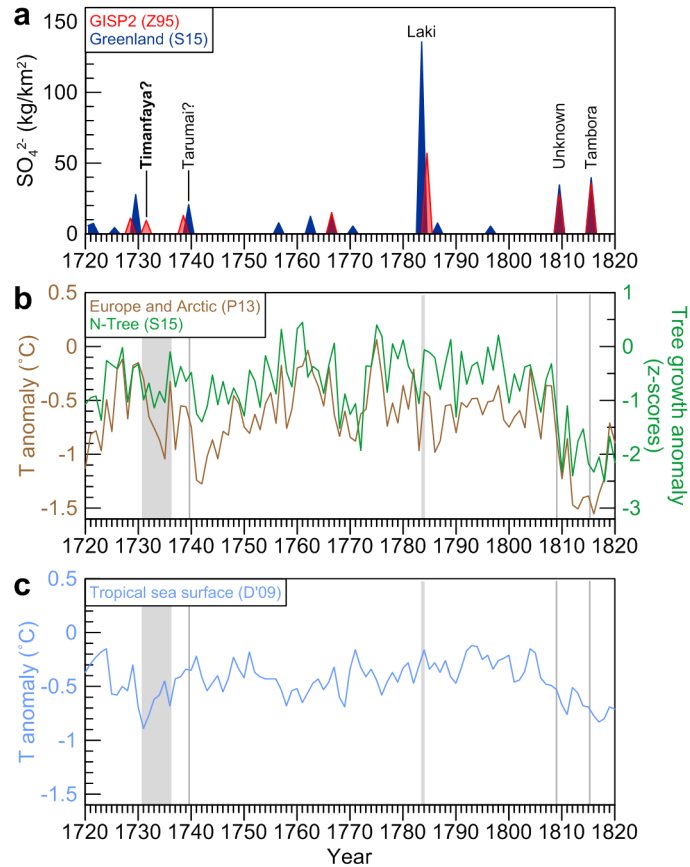


Figure 9. Paleoclimate records. (a) Sulfate anomalies in the Greenland ice sheet, from a single (Zielinski, 1995; Z95, red) and multiple ice cores (Sigl et al., 2015; S15, navy blue). Peaks associated with the 1815 Tambora eruption, 1809 unknown, and 1783–1784 Laki eruptions are labelled, along with anomalies possibly related to the 1739 VEI 5 eruption of Tarumai, Japan (Toohey & Sigl, 2017), and the 1730–1736 Timanfaya eruption. (b) Temperature anomaly for Europe and the Arctic (PAGES 2k Consortium, 2013; P13, brown) with respect to the 1961–1990 average and tree-ring growth anomalies relative to the 1000–1099 CE period from a Northern Hemisphere data composite (Sigl et al., 2015; S15, green). (c) Tropical sea surface temperature anomalies, with respect to the 1897–1981 period, from a multi-proxy reconstruction (D’Arrigo et al., 2009; D’09, light blue). The gray lines in panels (b) and (c) show the durations of the eruptions labelled in (a).